



Sedimentology of carbonate delta drifts

| | |
|-------------------------------|--|
| Journal: | <i>Sedimentology</i> |
| Manuscript ID | SED-2018-TP-115 |
| Manuscript Type: | Themed Issue Paper |
| Date Submitted by the Author: | 09-May-2018 |
| Complete List of Authors: | Reolid, Jesús; Universität Hamburg, Department of earth Sciences Betzler, Christian; Universität Hamburg, Department of Earth Sciences Lüdmann, Thomas ; Universität Hamburg, Department of earth Sciences Bohlen, Max; Universität Hamburg, Department of Earth Sciences |
| Keywords: | carbonate drift, siliciclastic drift, contourites, Maldives, Miocene |
| | |

Sedimentology of carbonate delta drifts

Jesús Reolid, Christian Betzler, Thomas Lüdmann, Max Bohlen

Abstract

The identification of sediment drifts typically relies on interpretation of reflection seismic data sets. Here, we sedimentologically analyze an example of a carbonate delta drift depositional system previously identified in seismics to provide a catalog of characteristic features at core and outcrop scale for allowing testing the occurrence of these poorly known type of deposit elsewhere. Cores and downhole logs recovered during IODP Expedition 359 to the Maldives in combination with seismic data were analyzed with this objective. The diagnostic criteria for the sedimentological recognition of a delta drift are: (1) the development of sigmoidal clinoforms that thin out towards proximal and distal settings, (2) proximal facies characterized by coarse-grained facies with abundant shallow-water components and distal facies dominated by fine-grained facies with rare to absent shallow-water components, (3) winnowing of the finer fraction in proximal facies, (4) extensive fragmentation of the bioclasts, (5) occurrence of large channels and bigradational intervals, and (6) the lobe to delta shaped outline of the sediment accumulation. The characteristic shallow-water fossil assemblage of the delta drift, which is Miocene in age, consists of large benthic foraminifera (*Amphistegina*, *Cycloclypeus*, *Lepidocyclina*, *Operculina*, *Heterostegina*), fragmented red algae and bryozoans, equinoid debris, and *Halimeda* plates. The deeper water part of the rift bodies consist of fine-grained planktonic foraminifera-rich wackestone. Condensed intervals may occur as result of enhanced bottom-current activity. In contrast to siliciclastic drift bodies, a carbonate delta drift has an important contribution by in-situ shallow-water carbonate production, which is proposed as a major controlling factor as important as the pelagic settling or the shaping by density and bottom currents in siliciclastic

1
2
3 drifts. In the absence of three-dimensional data and in two-dimensional views the carbonate
4
5 delta drift sediment bodies resemble carbonate ramps, which indicates that there may be the
6
7 need to re-evaluate various cases of such systems described from the geological record.
8
9

10
11 Keywords: carbonate drift, siliciclastic drift, contourites, Maldives, Miocene
12
13

14 15 **Introduction**

16
17
18 Currents are an important factor in shaping the outline of carbonate platforms (Neumann and
19
20 Ball, 1970, Mullins et al., 1980; Betzler et al., 2009, 2014, 2016a, b; Isern et al., 2004; Eberli
21
22 et al., 2010; John and Mutti, 2005; Lüdmann et al., 2013, 2016). The physical transport
23
24 capacity of currents induces selective deposition as well as sediment winnowing and
25
26 redistribution. In areas of lower current velocity, extensive sediment drifts may form. The
27
28 external morphology and internal architecture of these deposits have been widely studied
29
30 leading to a synoptic classification of predominately siliclastic drifts (Stow et al., 2002a,b;
31
32 Hernández-Molina et al., 2008; Rebesco et al., 2014). In contrast, the knowledge about
33
34 carbonate drifts is limited and restricted to deposits either at the flanks of the banks as
35
36 periplatform drifts (Mullins and Neumann, 1979; Mullins et al., 1980; Betzler et al., 2014;
37
38 Chabaud et al., 2016), in seaways separating carbonate banks as detached drifts (Bergmann,
39
40 2004; Anselmetti et al., 2000; Lüdmann et al., 2016; Paulat et al., in press), or at the
41
42 downcurrent end of shallow passages dissecting carbonate banks as delta drifts (Lüdmann et
43
44 al., 2013, 2018).
45
46
47
48

49
50 In most of these cases, the identification of the sedimentary succession as sediment drift relies
51
52 on the interpretation of reflection seismic data sets, i.e. examples where the large-scale
53
54 geometry is imaged. Here we present a sedimentological study of the poorly known delta drift
55
56 depositional system providing a catalog of diagnostic features displayed in thin section to
57
58
59
60

1
2
3 outcrop scale. Our results provide an overview on a delta drift and allow testing the
4
5 occurrence of such deposits elsewhere. Cores and downhole logs recovered during IODP
6
7 Expedition 359 to the Maldives allow an integrative characterization of the newly discovered
8
9 delta drift; and in addition, to address the diagnostic elements sharing or rather separating
10
11 carbonate and siliciclastic drifts.
12

13 14 15 **General setting and background**

16
17 The Maldives archipelago is an isolated carbonate platform in the Indian Ocean located to the
18
19 southwest of India and Sri Lanka (Fig. 1). A double row of atolls delineates the up to 500 m
20
21 deep Inner Sea basin which is connected to the open Indian Ocean by inter-atoll channels.
22
23 This modern structure of the Maldives is the latest stage of a dynamic geological evolution of
24
25 a carbonate edifice from the Paleocene to the present (Duncan and Hargraves, 1990; Aubert
26
27 and Droxler, 1992; Purdy and Bertram, 1993; Belopolsky and Droxler, 2003). The modern
28
29 platform configuration was achieved during the late Middle Miocene at ~13 Ma with atoll
30
31 growth paralleled by partial bank drowning and drift deposition (Purdy and Bertram, 1993;
32
33 Aubert and Droxler, 1996; Betzler et al., 2009, 2013, 2016b; Lüdmann et al., 2013). This
34
35 transition from a sea-level to current-controlled system was attributed to the onset and/or
36
37 intensification of the Indian monsoon that remains till present day (Betzler et al., 2009, 2013,
38
39 2016, 2017; Lüdmann et al., 2013; Reolid et al., 2017; Bunzel et al., 2017). Since the Middle
40
41 Miocene the Inner Sea was gradually infilled by ten mega sequences comprised of delta drifts,
42
43 elongated mounded drifts, and clinoform drift bodies (Lüdmann et al., 2013, 2018). The
44
45 middle to upper Miocene delta drifts that exhibit a delta-like geometry comprised of stacked
46
47 prograding clinoformal lobes are in the focus of this study.
48
49
50
51
52
53

54 **Methods**

55
56
57
58
59
60

1
2
3 This study is based on thin sections, reflection seismic data, and downhole logs from IODP
4 Exp. 359 hole U1466A (4°55.9880'N; 73°1.6894'E) and hole U1468A (4°55.98'N; 73°4.28'E)
5 (Betzler et al., 2017, 2018). Core retrieval, handling, and all on board measurements including
6 downhole logging and core to seismic correlation are described in detail in Betzler et al.
7 (2017).
8
9

10
11
12
13 The two IODP holes U1466A and U1468A were systematically sampled for detailed
14 microfacies analysis from core U1466A-12F to 50X and U1468A-32F to 63X, respectively
15 (Figs. 6 and 7). Usually two 10-cc oriented sample were taken per facies per core. A total of
16 147 thin sections were prepared out of these samples, 60 for hole U1466A and 87 for hole
17 U1468A. Grain size was visually defined on-board according to the Wentworth-Udden scale
18 for carbonate rocks. In the case of Site U1466A there is an additional mean wt% grain size
19 distribution calculated out of wet sieved samples using the weighted arithmetic mean. The
20 physical properties and downhole logs used are Natural Gamma Radiation (NGR), Total
21 Gamma Ray (HSGR), as well as the elemental abundance of U, K, and Th obtained of the
22 Spectral Gamma Radiation (HNGS). Reflection seismic data were acquired during the R/V
23 Meteor cruise M74/4 and R/V Sonne SO-236 using a Hydroscience Technologies Inc. 144
24 channel digital streamer array. The streamer had an active length of 600 m and an asymmetric
25 group interval between 0.5 and 6.25 m. Seismic signals were generated by two clustered GI-
26 Guns of 45 in³ in volume for a 105-in³ generated injector volume. The dominant frequencies
27 were 100 to 120 Hz. A distance-controlled shooting interval of 25 m was used. The data were
28 processed with the Promax software package (Halliburton-Landmark) to zero phase, filtered
29 in time and f-k domain, and corrected for dip and normal moveout. The predictive
30 deconvolution of the pre-stacked data successfully removed the water bottom multiple in
31 basinal areas. Finally, a migration was carried out in time domain. Interpretation and
32 visualization was done using the software package Petrel (Schlumberger). Sequence
33 boundaries were previously defined in Lüdmann et al. (2013, 2018). Sequence boundaries are
34
35
36
37
38
39
40
41
42
43
44
45
46
47
48
49
50
51
52
53
54
55
56
57
58
59
60

1
2
3 numbered from DS1 to DS10, the sequence overlying the corresponding boundaries are
4
5 termed ds1 to ds10.
6
7

8 9 **Results**

10 11 **Seismic stratigraphy and facies**

12
13 The deposits studied herein are attributed to sequences ds1 and ds2 (Lüdmann et al., 2013).
14
15 These are the oldest sequences overlying the ~13 Ma drowning unconformity and differ from
16
17 the underlying platform sequences with concave-up clinoform bodies by their convex-up
18
19 shape (Lüdmann et al., 2013; Fig. 2) and lobate geometry in outline which defines them as
20
21 delta drifts (Lüdmann et al., 2018).
22
23

24
25 In W-E seismic sections, ds1 and ds2 thin out towards the Inner Sea basin (Fig. 2). An erosive
26
27 trough-shaped depression truncates the drift body at its proximal end in the central part of the
28
29 Northern Kardiva Channel (Betzler et al., 2013; Lüdmann et al., 2013, 2018). The depression
30
31 infill is characterized by discontinuous reflections of medium to low amplitude. Laterally, the
32
33 erosion is limited (Fig. 3). The drift deposits of ds1 onlap the talus slope of the drowned
34
35 platform, while the deposits of ds2 directly onlap the sequence boundaries DS1 and DS2 (Fig.
36
37 3). In N-S seismic sections, the drift body is characterized by subhorizontal reflection bundles
38
39 (Fig. 4 and 5). According to the internal reflection pattern and the seismic facies analysis
40
41 (based on concepts of Mitchum et al., 1977) summarized in Table 1, ds1 and ds2 can be
42
43 divided into a total of 5 subsequences. Accordingly, drift sequence ds1 is composed of
44
45 subsequences 1a, 1b, and 1c. Subsequence 1a is bounded at its base and top by DS1/DS1A
46
47 and DS1B, respectively and has a concave upward geometry (Fig. 2). Subsequence 1b of Drift
48
49 Sequence 1 is a wedge shaped body with sigmoidal clinoforms (Fig. 2). Subsequence 1c is
50
51 also wedge shaped and represents the progradation of the sigmoidal clinoforms toward the
52
53 basin interior. Drift sequence ds2 exists of subsequences 2a and 2b. Subsequence 2a is
54
55 bounded at its base and top by DS2/DS2A and DS2B, respectively and is characterized by
56
57
58
59
60

1
2
3 subparallel reflections in N-S profiles. Subsequence 2b is bounded at its base and top by
4 DS2B and DS3, respectively. It reveals a mound-like shape and reflections that onlap DS2B
5 in N-S profiles.
6
7
8
9

11 **Depositional Sequences**

12
13 The depositional sequences in holes U1466A and U1468A were defined by combining
14 seismic facies (Table 1), microfacies analysis (Table 2), and HSGR log characteristics (Figs.
15 6, 7). Changes in the content of large benthic foraminifera (LBF) were especially helpful to
16 identify sequence boundaries. The depositional sequences coincide with the sequences and
17 subsequences determined in the seismic interpretation and are therefore named after the
18 seismic sequences.
19
20
21
22
23
24
25
26
27

28 Drift Sequence 1a (ds1a)

29
30
31 Depth 311-162 mbsf (U1466A)

32
33 428-408 mbsf (U1468A)

34
35 In its lower part, ds1a exhibits subparallel reflections (SF2; Tab. 1) that onlap DS1A (Fig. 3).
36
37 In N-S direction the reflections are subhorizontal and gradually change from SF5 to SF6 (Fig.
38 4 and 5; Tab. 1). Reflection amplitude increases basinwards as reflections converge (SF3 and
39 SF6; Tab. 1) and overall thickness of the sequence decreases (Fig. 3). The sediment in this
40 interval is dominated by a coarse-grained foraminiferal packstone (Fig. 8a). A distinctive
41 interval rich in LBF and planktonic foraminifera occurs at 290 to 278 mbsf, otherwise LBF
42 are rare. In downhole logs, the bottom part of ds1a is characterized by average HSGR values
43 of 25 gAPI and (Fig. 6). An interval from 294 to 268 mbsf of higher HSGR (~36 gAPI)
44 coincides with the interval rich in LBF (278- 290 mbsf).
45
46
47
48
49
50
51
52
53

54 The middle part of ds1a, between 240-200 mbsf, is characterized by sigmoidal to oblique
55 progradational clinofolds (SF1; Tab.1) that thin out towards the basin with bottomsets
56
57
58
59
60

1
2
3 terminating in downlaps with wavy patterns (SF4; Tab. 1) (Fig. 3). The steep side of these
4 waves, previously interpreted as cyclic steps (Lüdmann et al., 2018) is directed upslope. In
5 intersecting lines P38 and P23 seismic facies grade from SF5 to SF6 towards the basin (Fig. 4
6 and 5; Tab. 1). The facies of this interval consists of bioclastic packstone from 242 to 216
7 mbsf and fine grained wackestone from 216 to 200 mbsf (Fig. 8b). The average grain size is
8 63 – 250 μm and displays a fining upward trend. The matrix of the fine grained materials
9 consists of micrite made up of calcareous nannofossils and aragonite needles. Typical HSGR
10 values are around 25 gAPI with maximum amplitudes of 4 gAPI
11

12 From 200 mbsf to its top, ds1a is characterized by sigmoidal clinoforms with subparallel
13 reflections that converge and gradually change from seismic facies SF2 in the proximal area
14 to SF4 towards the basin (Fig. 2; Tab. 1). In intersecting line P38 reflections grade from SF5
15 at Site U1468 to SF6 to the north and south (Fig. 4; Tab. 1). The facies in this interval consists
16 of organic-rich wackestone interbedded with partially lithified to lithified intervals of
17 bioclastic packstone (Table 2, Fig. 6). The grain size average is 63-250 μm . From the lower
18 boundary of the sequence, the HSGR increases from around 18 gAPI to 39 gAPI at 176 mbsf
19 and exhibits high amplitudes of up to 10 gAPI. Partially lithified to lithified intervals have
20 higher HSGR values. Above 172 mbsf, HSGR decreases to 19 gAPI (162 mbsf) with
21 amplitudes in the range of 5 to 8 gAPI. The upper boundary of ds1a is DS1B (Fig. 2).

22 Drift Sequence 1a at U1468A consists of very-fine grained bioclastic packstone that
23 correspond to SF4 which represents the cyclic steps (Fig. 2; Tab. 1). The sediment is intensely
24 bioturbated but not totally homogenized. HSGR values range between 20 gAPI and 30 gAPI
25 (Fig. 7).

26
27
28
29
30
31
32
33
34
35
36
37
38
39
40
41
42
43
44
45
46
47
48
49
50
51
52 Drift Sequence 1b (ds1b)

53
54
55 Depth 163-96 mbsf (U1466A)

56
57
58
59
60 408-270 mbsf (U1468A)

1
2
3 Drift Sequence 1b overlies seismic horizon DS1B and is a lobe with progradational-sigmoidal
4
5 clinoforms (SF1) (Fig. 3; Tab. 1). Continuity and amplitude of reflections are low (SF7) but
6
7 gradually increase towards the basin (SF3) (Fig. 3; Tab. 1). Reflections in the proximal
8
9 intersecting line P38 are semi-continuous (SF5) whereas reflections at the basinal line P23 are
10
11 continuous and of high-amplitude in P23 (SF6) (Fig. 4 and 5; Tab. 1). The facies of the
12
13 proximal part of ds1b consists of a *Cycloclypeus* wackestone which changes upcore into the
14
15 LBF-rich facies at 129 mbsf at Site U1466A (Fig. 8c). The LBF-rich facies display an
16
17 alternation of fragmented LBF packstone, nummulitid packstone, and *Amphistegina*
18
19 *grainstone* at the top (Fig. 8d-f). There are a total of three of such packages at Site U1466
20
21 to 13 m thick, with each one characterized by cycles of coarsening and fining upward. The
22
23 HSGR values are relatively stables, and with values of 17 gAPI to 25 gAPI (Fig. 6) in average
24
25 lower than in the previous sequences. The upper boundary of ds1b is eroded at this location
26
27 (Fig. 2).
28
29

30
31 Erosive channels are a distinctive feature of this subsequence and occur in both intersecting
32
33 lines (Lüdmann et al., 2018), though they are more abundant at the distal Site U1468 (Fig. 5).
34
35 Channels incise underlying reflections as indicated by truncations (Figs. 4, 5). The subsequent
36
37 channel infill consists of a dominantly aggradational pattern of the reflections. In line P23
38
39 these downlapping reflections grade into trough-shaped reflections towards the top. Some
40
41 reflections simultaneously terminate in downlaps and truncations as observed in line P23 (Fig.
42
43 5). Channels are stationary.
44
45

46
47 High-amplitude bottomsets (SF3) at Site U1468 can be correlated to an alternation of chert-
48
49 nodule packstone and sponge spicule-bryozoan packstone in cores (Fig. 9a-b; Tab. 1). The
50
51 subsequence is characterized by relatively stable HSGR measurements around 15 gAPI. The
52
53 top of ds1b is eroded at Site U1466 and bounded by DS1C at 270 mbsf at Site U1468.
54
55

56
57 Drift Sequence 1c (ds1c)
58
59
60

1
2
3 Depth 270-197 mbsf (U1468A)

4
5 The lower boundary of ds1c is the turnover from seismic facies SF3 of the underlying
6
7 subsequence to SF7 (Tab. 1), and also the abandonment of parts of the channel system (Fig.
8
9 5). This turnover is characterized by an abrupt increase of the HSGR (Fig. 3 and 7). In W-E
10
11 direction ds1c is wedge-shaped with relatively thin topsets, though overall thickness increases
12
13 towards the basin (Fig. 2). Reflections of the topsets grade from SF7 to SF8 towards the basin
14
15 (Tab. 1). In N-S direction, reflections are discontinuous and of low amplitude (SF5; Tab. 1)
16
17 (Fig. 5). A channel (SF9; Tab. 1), was still active to the north of Site U1468 during formation
18
19 of this unit. The prevailing sedimentary facies are the sponge spicule-bryozoan packstone and
20
21 the fragmented LBF packstone. The abundance of LBF increases towards the top of the
22
23 subsequence (Fig. 7). The values of the HSGR log are between 15 and 23 gAPI (Fig. 7). The
24
25 upper boundary of ds1c is the base of the overlying ds2.
26
27
28
29

30
31 Drift Sequence 2a (ds2a)

32
33 Depth 197-135 mbsf (U1468A)

34
35 Drift sequence 2a is characterized by subparallel reflections that onlap DS2A and diverge
36
37 toward the basin (SF7; Tab. 1). The reflections progressively steepen and become chaotic
38
39 towards the basin (Fig. 2). In N-S direction the reflections are parallel and of relatively high
40
41 amplitude (SF6; Tab. 1) (Fig. 5). The reflections are slightly mounded and onlap the
42
43 underlying parallel reflections (Fig. 5). The thickness of this subsequence faintly decreases
44
45 with increasing distance from Site U1468 (Fig. 5). The sedimentary facies of ds2a consists of
46
47 a *Lepidocyclina* packstone alternating first with nummulitid packstone and continuing upcore
48
49 with *Amphistegina* packstone to grainstone (Fig. 9c). The NGR values range from 8 cps to 30
50
51 cps, with a base level around 12 cps. The HSGR displays average values of 17 gAPI and
52
53 fluctuations between 10 gAPI and 25 gAPI. The upper boundary of ds2a marks the sequence
54
55 boundary DS2B.
56
57
58
59
60

1
2
3
4
5 Drift Sequence 2b (ds2b)

6
7 Depth 135-60 mbsf (U1468A)

8
9 Drift sequence 2b is characterized by subparallel reflections that onlap the surface DS2B in
10 line P65 (Fig. 2). The reflections, like those of ds2a, progressively steepen and become
11 chaotic towards the basin (Fig. 2). In N-S direction the reflections are sub-parallel and of
12 chaotic towards the basin (Fig. 2). In N-S direction the reflections are sub-parallel and of
13 medium- to low-amplitude with chaotic reflections to the north of Site U1468 becoming
14 subparallel to the south (SF5 to SF6; Tab. 1; Fig. 5). The reflections have a mound-like
15 configuration thinning out to the north and the south of the borehole, respectively (Fig. 5).
16 Between 120 and 110 mbsf and at 75 mbsf there are intervals of *Halimeda* grainstone to
17 packstone (Fig. 9d). The *Lepidocyclina* packstone is rare in this sequence and there is an
18 alternation of *Amphistegina* packstone, nummulitid packstone, and fragmented LBF
19 packstone similar to that of ds1b (Fig. 9e). The hole conditions did not allow the operation of
20 the downhole logging tools and accordingly there are no HSGR logs available (Fig. 7). NGR
21 data, measured at the cores show the highest differences in amplitude of up to 25 cps and an
22 overall increase from 8 cps at 116 mbsf to 45 cps at 84 mbsf. The upper boundary of ds2b is
23 the sequence boundary DS3.
24
25
26
27
28
29
30
31
32
33
34
35
36
37
38
39
40

41 **Discussion**

42 The sedimentary facies variations together with changes of the seismic facies and geometries,
43 as well as the downhole log characteristics were used for an interpretation of the carbonate
44 delta drift in terms of hydrodynamic energy, reworking, and paleobathymetry. The latter is
45 mainly based on the LBF associations.
46
47
48
49
50
51

52 **Paleoenvironmental Interpretation**

53
54
55
56
57
58
59
60

1
2
3 The facies association of foraminiferal packstone, bioclastic packstone, mud-rich bioclastic
4 wackestone, and organic-rich wackestone of subsequence ds1a was deposited in a relative
5 deep environment affected by currents that winnowed and sorted the sediment. Cyclic steps
6 are characteristic of this subsequence and were produced by density flows likely triggered by
7 currents flowing over the platform top to the basin (Lüdmann et al., 2013, 2018). The
8 occurrence of such phenomena is in line with the occurrence of some reworked shallow-water
9 components coralline algae and large benthic foraminifera at the base of ds1a at U1466A. The
10 sediment related to the density flows originally inherited the concave-upward slope geometry
11 of the underlying platform slope clinoforms, but progressively the sediment exported into the
12 basin adopted the convex-upward equilibrium profile characteristic of the drift, which is
13 reflected by a change from subparallel to sigmoidal-oblique clinoforms prograding
14 basinwards (Fig. 2). Current intensity was variable as indicated by the bigradational sorting of
15 the bioclasts (Fig. 6). The bigradational sorting is a typical diagnostic criteria of the action of
16 bottom currents (Stow et al., 2002a,b; Hüneke and Stow, 2008; Stow and Faugères, 2008), but
17 it may occur also related to high-density grain flows that developed a traction carpet such as
18 hyperpycnal flows (Lowe, 1982; Mulder et al., 2003). Hyperpycnal flows may occur in the
19 marine environment when river discharge enters the ocean with a high concentration of
20 suspended materials (Mulder et al., 2003), or when high-density flows from carbonate
21 platform internal areas reach down to the platform slopes (Betzler et al., 2014; Schnyder et al.,
22 2018). In the Maldives there was a different setting at the time of cyclic step formation with
23 the Kardiva Channel connecting the Indian Ocean with the Inner Sea (Betzler et al., 2013;
24 2016; Lüdmann et al., 2013, 2018). The currents flowing through this passage, rich in
25 suspended materials from the platform top, are proposed, when dense enough, to trigger the
26 downslope flows producing cyclic steps at the distal slope.

27
28
29
30
31
32
33
34
35
36
37
38
39
40
41
42
43
44
45
46
47
48
49
50
51
52
53
54
55 The partially lithified intervals with some shallow water components such as coralline algae at
56 the top of subsequence ds1a are interpreted as condensed intervals which formed at times of
57
58
59
60

1
2
3 sea floor sediment winnowing. These condensed intervals are enriched in organic matter such
4
5 as fish remains and particulate organic matter. This corresponds to high values of HSGR log
6
7 and NGR by high values at the condensed intervals. High HSGR and NGR values in the
8
9 Maldives have been proved to indicate high organic-matter content (Betzler et al., 2016b,
10
11 2018; Reolid and Betzler, 2018).

12
13 The lower part of ds1b is marked by the occurrence of a mud-rich *Cycloclypeus* wackestone
14
15 with abundant planktonic foraminifera and rare unidentifiable bioclasts (Fig. 6). The tests of
16
17 *Cycloclypeus* specimens are very thin but well preserved which is interpreted to reflect little
18
19 to scarce transport of components (Fig 8c). Chaproniere (1975) reported *Cycloclypeus* to
20
21 dwell from 50 m water depth to the base of the photic zone at ~120 m, this lower limit of
22
23 distribution is supported by Hohenegger (1999). Thus *Cycloclypeus* are interpreted as
24
25 autochthonous to para-autochthonous at best, which places the deposition of ds1b in the
26
27 middle to lower part of the photic zone.
28
29

30
31 At Site U1466, a facies change from the *Cycloclypeus* wackestone to the fragmented LBF
32
33 packstone at 130 mbsf indicates a shallowing of the environment with progressively more
34
35 LBF and less planktonic foraminifera (Fig. 6). The fragmented LBF packstone is
36
37 characterized by locally abundant bioclasts and a mud-poor silt-sized microgranular matrix
38
39 which is interpreted to indicate a more energetic environment compared to the *Cycloclypeus*
40
41 wackestone facies (Fig. 8d). The overlying nummulitid packstone is dominated by
42
43 *Cycloclypeus* and *Operculina* that according to Tsuji (1993) and Hohenegger et al. (1994)
44
45 prefer low-to medium-energy settings. This interpretation is in line with the reduction in
46
47 abundance of silt-sized bioclasts in this facies with respect to the underlying fragmented LBF
48
49 packstone. The simultaneous occurrence of two relatively deeper dwelling LBF like
50
51 *Operculina* and *Cycloclypeus* indicates that the nummulitid packstone represents a deeper and
52
53 less energetic paleoenvironment than the fragmented LBF packstone. The overlying
54
55 *Amphistegina* packstone to grainstone is dominated by two species of *Amphistegina*, *A.*
56
57
58
59
60

1
2
3 *lobifera* and *A. lessonii*. The lense-shaped *A. lobifera* is reported to dwell in water depths of 0-
4 12 m (Renema and Troelstra, 2001) or 0-35 m (Hohenegger, 2000) with a maximum depth of
5 <40 m (Hansen and Buchardt, 1977). The *A. lessonii* is flatter and prefers slightly deeper
6 environments of up to 40 m (Renema and Troelstra, 2001) to 50 m (Hohenegger, 1999). Both
7 species of *Amphistegina* are diagnostic of seagrass meadows that elsewhere occur from the
8 shore to the lower inner ramp (Mateu-Vicens et al., 2009). The occurrence of large allochems
9 including large benthic foraminifera and fragmented coralline red algae indicates a shallow
10 environment with relatively high hydrodynamic energy (Fig. 8f).

11
12
13
14
15
16
17
18
19
20 The hydrodynamic energy of the bottom currents was likely lower than at the time of the
21 deposition of the nummulitid packstone as deduced by the decrease in the amount of silt-sized
22 bioclast, but it was still significant as deduced from features as the coarsening- and fining-
23 upward cycles observed in this interval (Fig. 6). Under this perspective, the alternation of the
24 LBF-rich facies at Site U1466 may be interpreted as a combination of base-level fluctuations
25 and changes in the intensity of the currents affecting the carbonate factory with the shallowest
26 environment represented by the *Amphistegina* packstone to grainstone and the deepest by the
27 fragmented LBF packstone. In contrast, the most energetic environment is represented by the
28 fragmented LBF packstone, while the nummulitid and *Amphistegina* packstone were likely
29 deposited under slightly weaker current conditions.

30
31
32
33
34
35
36
37
38
39
40
41
42 In addition to the compositional and textural variations, the seismic facies drastically changes
43 from ds1a to ds1b (Fig. 4 and 5). The cyclic steps of ds1a disappear in ds1b, which is in-line
44 with a decay of the bottom current energy (Fig. 2). In contrast, large channels occur in the
45 carbonate delta drift throughout ds1b, best seen in the strike parallel lines (Fig. 4 and 5).
46 These channels are linear features as they occur in a similar position along consecutive
47 parallel seismic lines (Fig. 4 and 5, Lüdmann et al., 2013, 2018). The infill pattern of the
48 channels, with superimposed trough-like reflections, indicates that the channels persisted
49
50
51
52
53
54
55
56
57
58
59
60

1
2 throughout the formation of ds1b which is in line with the interpretation of a prevailing W-E
3 bottom-current regime (Fig. 5).
4

5
6 At the distal Site U1468, the cyclic alternation of chert-nodule packstone and sponge spicule-
7 bryozoan packstone may represent the basinal equivalent of the alternation observed in the
8 LBF-rich facies of the proximal area (Fig. 2). This will remain hypothetical, as the proximal
9 part of this delta drift interval, i.e. the westernmost part of ds1b is not preserved in line P65,
10 which crosses IODP site U1466 and U1468, because deposits were eroded presumably during
11 formation of DS3 (Fig. 2). To the south, in Line P32 (Fig. 3), ds1b wedges out against the
12 relief of the drowned carbonate bank.
13
14
15
16
17
18
19
20
21

22 Sequence ds1c is only preserved east of Site U1466 (Fig. 2). The faunal assemblage of ds1c at
23 Site U1468 is comparable to the LBF-rich facies in sequence ds1b at Site U1466 indicating
24 deposition in a shallow environment with respect to ds1b (Fig. 7). This is interpreted to reflect
25 a migration of the shallow-water facies belt towards the Inner Sea from the position of U1466
26 to that of U1468 throughout the growth of the delta drift. The alternation of LBF-rich facies in
27 the overlying ds2 may be either interpreted as changes in the water depth and/or intensity of
28 the currents as the amount of planktonic foraminifera and reworked bioclast fluctuates from
29 one facies to the next (Fig. 9). The reduced amount of *Operculina* with respect to the
30 corresponding facies at U1466 is consistent with an environment of increased hydrodynamic
31 energy (Tsuji, 1993; Hohenegger et al., 1994). Further, the hydrodynamic energy of the
32 environment apparently increased towards the top of ds2 with abundant coarse-grained
33 grainstone where encrusting organisms such as red algae, bryozoan, and encrusting
34 foraminifera are especially abundant (Fig. 7). The *Halimeda* grainstone of ds2b likely
35 represents the shallower facies in the succession (Fig. 9).
36
37
38
39
40
41
42
43
44
45
46
47
48
49
50
51
52
53

54 **Sedimentology of carbonate delta drift deposits**

55
56
57
58
59
60

1
2
3 Based on seismic scale depositional geometries it has previously been shown that the herein
4 studied sediment package has been formed by eastward directed bottom currents, which were
5 flowing through channels and passages sculptured in a drowned carbonate bank (Betzler et al.,
6 2013; Lüdmann et al., 2013, 2018). This interpretation is now amended by a herein presented
7 extensive sedimentological dataset, which allows linking the seismic scale to the core and
8 outcrop scale. In particular, there are distinctive sedimentological evidences that indicate the
9 current control on deposition including (1) large channels (Fig. 4 and 5) in subsequences ds1b
10 and ds1c, and (2) intensely reworked bioclasts.

11
12
13
14
15
16
17
18
19
20 The continuous reworking of sediment by the persistent action of currents is a diagnostic
21 criterion for drifts deposits (Stow et al., 2002a; Rebesco et al., 2014). Condensed intervals
22 occurring in ds1a are also typical of drift deposits, where the currents are temporally
23 intensified causing winnowing at the sea floor (Fig. 10) (Hüneke and Stow, 2008). The
24 absence of distinct lamination and the complete homogenization of the sediment by intense
25 bioturbation are also typical of drift deposits according to Hüneke and Stow (2008), Stow and
26 Faugères (2008), and Rebesco et al. (2014).

27
28
29
30
31
32
33
34
35 The filling of the accommodation by the aggrading to prograding delta drift system was not
36 exclusively the result of the accumulation of current-transported sediment, but also caused by
37 in-situ carbonate production of a middle- to shallow-water assemblage (i.e. *Cycloclypeus* at
38 the base of ds1b). Progressive infill of accommodation and shallowing of the sea-floor is
39 reflected by the establishment of shallow water assemblages (i.e. *Amphistegina* packstone to
40 grainstone) at the apex of the drift body (Fig. 10). In ds2, a shallow-water paleoenvironmental
41 setting is evidenced by the dominance and diversity of large benthic foraminifera and the
42 occurrence of coralline algae and *Halimeda* in ds2 (Fig. 9d). These components only show
43 little evidence of reworking indicating that towards the top of the delta drift succession, in-situ
44 carbonate production dominated over current action, or at least was more important compared
45 to the lower part of the delta drift succession (Fig. 11).

46
47
48
49
50
51
52
53
54
55
56
57
58
59
60

1
2
3 The possibility of a coinciding bottom current reworking and in-situ carbonate production is a
4 unique feature of carbonate delta drifts and has not been previously reported from drift
5 deposits elsewhere. Similarly, Rebesco et al. (2014) postulated a multi-process evolution for
6 siliciclastic sediment drifts that are not exclusively the product of bottom currents but the
7 result of the interplay of (1) bottom currents, (2) pelagic settling, and (3) density currents (Fig.
8 11). In the carbonate delta drift these controlling factors are represented by the winnowing of
9 sediment in the condensed intervals and the occurrence of intensely reworked bioclasts by
10 bottom currents, the pelagic settling of micrite and planktonic foraminifera, and the
11 occurrence of cyclic steps as the result of density currents. In addition to these three
12 controlling factors, the facies of the drift deposits of the Maldives show that in-situ carbonate
13 production is a fourth and additional factor to take into account for the formation of such
14 sediment bodies (Fig. 11).
15
16
17
18
19
20
21
22
23
24
25
26
27
28
29
30

31 **CONCLUSIONS**

32
33 For the first time, a sedimentological characterization of carbonate delta drifts is introduced.
34
35 In contrast to siliciclastic drift bodies, this carbonate sediment drift system has an important
36 contribution by shallow-water in-situ carbonate production. It is proposed that this in-situ
37 carbonate production is a control factor of drift bodies as important as the pelagic settling or
38 the shaping by density and bottom currents.
39
40
41
42

43
44 The overall geometry of the delta drift consists of sigmoidal clinoforms that thin out towards
45 proximal and distal settings. The diagnostic criteria for the sedimentological recognition of a
46 delta drift are the followings:
47
48
49

- 50 (1) The facies assemblage changes from proximal to distal settings. Proximal settings are
51 characterized by coarse-grained facies with abundant shallow-water components. The
52 distal setting is dominated by fine-grained facies with rare to absent shallow-water
53 components.
54
55
56
57
58
59
60

- 1
2
3 (2) Proximal facies belts of the delta drift are characterized by the winnowing of the micrite
4
5 in contrast to the distal facies.
6
7 (3) The distinctive fossil assemblage of the delta drift is of shallow water. The main
8
9 components are large benthic foraminifera (*Amphistegina*, *Cycloclypeus*, *Lepidocyclina*,
10
11 *Operculina*, *Heterostegina*), fragmented red algae and bryozoans, equinoid debris, and
12
13 *Halimeda* plates.
14
15 (4) Fragmentation of the bioclasts is intense.
16
17 (5) Large channels and bigradational intervals are representative sedimentary structures of
18
19 the delta drift.
20
21 (6) Bioturbation is intense and mask most of the sedimentary structures.
22
23 (7) The delta drift may present a transitional stage dominated by currents and gravity flows
24
25 (ds1a in the study case) that predates the establishment of the shallow water carbonate
26
27 factory in the delta drift. This transitional stage is characterized by cyclic steps and
28
29 reworked materials from shallower areas.
30
31 (8) Condensed intervals may occur as result of enhanced bottom-current activity.
32
33
34

35 We propose that the example of carbonate delta drift depositional systems described from the
36
37 Maldives archipelago is not singular. Similar settings and situations as in the Maldives are
38
39 given in many carbonate platforms, such as passages between individual banks or banks
40
41 covered by a shallow water column where current reworked sediments accumulate on the
42
43 downcurrent side of shallow banks. We therefore propose to critically test cases where similar
44
45 platform configurations were described. For example, in absence of a three-dimensional
46
47 control of the depositional geometries, a two-dimensional section of a carbonate delta drift
48
49 may be mistaken to present a ramp depositional system.
50
51
52
53

54 **Acknowledgements**

55
56
57
58
59
60

1
2
3 We acknowledge funding by the DFG through grant Be 1272/23-1 and -2. Many discussions
4 with the IODP Exp. 359 shipboard scientists helped us to sharpen our concept; special thanks
5 go to Gregor Eberli. Additional acknowledgements go to the companies HALLIBURTON-
6 LANDMARK, SCHLUMBERGER and CEGAL Geosciences for providing university grants
7 for the seismic processing software PROMAX and seismic interpretation software PETREL
8 as well as its BLUEBACK plugin. Eva Vinx is thanked for the production of the many thin
9 sections.
10
11
12
13
14
15
16
17
18
19

20 **References**

21
22 Anselmetti, F.S., Eberli, G.F. and Ding, Z.D. (2000) From the Great Bahama Bank into the
23 Straits of Florida: A margin architecture controlled by sea-level fluctuations and ocean
24 currents. *Geol. Soc. Am. Bull.*, **112**, 829-844.
25
26
27
28
29

30
31
32 Aubert, O. and Droxler, A.W. (1992) General Cenozoic evolution of the Maldives carbonate
33 system (equatorial Indian Ocean). *Bull. Centres Rech. Explor.-Prod. Elf-Aquitaine*, **16**, 113-
34 136.
35
36
37
38
39

40
41
42 Aubert, O. and Droxler, A.W. (1996) Seismic stratigraphy and depositional signatures of the
43 Maldivian Carbonate System (Indian Ocean). *Mar. Petrol. Geol.*, **13**, 503-536.
44
45
46
47
48

49
50 Belopolsky, A. and Droxler, A. (2003) Imaging Tertiary Carbonate System - the Maldives,
51 Indian Ocean: Insights into Carbonate Sequence Interpretation. *Lead. Edge*, **22**, 646-652.
52
53
54
55
56
57
58
59
60

1
2
3 *Bergman, K.L. (2004) Seismic analysis of paleocurrent features in the Florida Straits: insights*
4 *into the paleocurrent, upstream tectonics, and the Atlantic-Caribbean connection. Ph.D. thesis,*
5 *University of Miami, 190 pp.*
6
7
8
9

10
11
12
13 Betzler, C., Hübscher, C., Lindhorst, S., Reijmer, J.J.G., Römer, M., Droxler, A., Fürstenau, J.
14 and Lüdmann, T. (2009) Monsoon-Induced Partial Carbonate Platform Drowning (Maldives,
15 Indian Ocean). *Geology*, **37**, 867-870.
16
17
18
19

20
21
22
23 Betzler, C., Lüdmann, T., Hübscher, C. and Fürstenau, J. (2013) Current and Sea-Level
24 Signals in Periplatform Ooze (Neogene, Maldives, Indian Ocean). *Sed. Geol.*, **290**, 126-137.
25
26
27
28

29
30
31 Betzler, C., Lindhorst, S., Eberli, G.P., Lüdmann, T., Möbius, J., Ludwig, J., Schütter, I.,
32 Wunsch, M., Reijmer, J.J.G. and Hübscher, C. (2014) Periplatform drift: the combined result
33 of contour current and off-bank transport along carbonate platforms. *Geology*, **42**, 871-874.
34
35
36
37
38

39
40
41 Betzler, C., Eberli, G.P., Alvarez-Zarikian, C.A. and the Expedition 359 Scientists (2016a)
42 *Expedition 359 Preliminary Report: Maldives Monsoon and Sea Level. International Ocean*
43 *Discovery Program.* <http://dx.doi.org/10.14379/iodp.pr.359.2016>.
44
45
46
47
48

49
50
51 Betzler, C., Eberli, G.P., Kroon, D., Wright, J.D., Swart, P.K., Nath, B.N., Alvarez-Zarkikian,
52 C.A., Alonso-Garcia, M., Bialik, O.M., Blatter, C.L., Guo, J.A., Haffen, S., Horozal, S.,
53 Inoue, M., Jovane, L., Lanci, L., Laya, J.C., Mee, A.L., Lüdmann, T., Nakakuni, M., Niino,
54
55
56
57
58
59
60

1
2
3 K., Petruny, L.M., Pratiwi, S.D., Reijmer, J.J.G., Reolid, J., Slagle, A.L., Sloss, C.R., Su, X.,
4 Yao, Z. and Young, J.R. (2016b) The Abrupt Onset of the Modern South Asian Monsoon
5 Winds. *Scientific Reports*, **6**, 29838.
6
7
8
9

10
11
12 Betzler, C., Eberli, G.P., Alvarez-Zarikian, C.A., and the Expedition 359 Scientists, 2017.
13 *Maldives Monsoon and Sea Level*. Proceedings of the International Ocean Discovery
14 Program, 359: College Station, TX (International Ocean Discovery Program).
15 <http://dx.doi.org/10.14379/iodp.proc.359.2017>
16
17
18
19
20
21
22

23
24
25 Betzler, C., Eberli, G.P., Lüdmann, T., Reolid, J., Kroon, D., Reijmer, J.J.G., Swart, P.K.,
26 Wright, J., Young, J.R., Alvarez-Zarikian, C., Alonso-García, M., Bialik, O.M., Blättler, C.L.,
27 Guo, J.A., Haffen, S., Horozal, S., Inoue, M., Jovane, L., Lanci, L., Laya, J.C., Hui Mee, A.L.,
28 Nakakuni, M., Nath, B.N., Niino, K., Petruny, L.M., Pratiwi, S.D., Slagle, A.L., Sloss, C.R.,
29 Su, X. and Yao, Z. (2018) Refinement of Miocene sea-level and monsoon events from the
30 sedimentary record of the Maldives (Indian Ocean). *Progress in Earth and Planetary Science*.
31 DOI 10.1186/s40645-018-0165-x
32
33
34
35
36
37
38
39
40
41
42

43
44 Bunzel, D., Schmiedl, G., Lindhorst, S., Mackensen, A., Reolid, J., Romahn, S., Betzler, C.
45 (2017) A multi-proxi analysis of Late Quaternary ocean and climate variability for the
46 Maldives, Inner Sea. *Clim. Past*, **13**, 1791-1813. <https://doi.org/10.5194/cp-13-1791-2017>
47
48
49
50
51
52

53
54 Chabaud, L., Ducassou, E., Tournadour, E., Mulder, T., Reijmer, J.J.G., Conesa, G.,
55 Giraudeau, J., Hanquiez, V., Borgomano, J. and Ross, L. (2016) Sedimentary processes
56
57
58
59
60

1
2
3 determining the modern carbonate periplatform drift of Little Bahama Bank. *Mar. Geol.*, **378**,
4
5 213-229.
6
7

8
9
10 Chaproniere, G.C. (1975) Palaeoecology of Oligo-Miocene larger Foraminiferida, Australia.
11
12 *Alcheringa*, **1**, 37-58.
13
14

15
16
17
18 Duncan, R.A. and Hargraves, R.B. (1990) $^{40}\text{Ar}/^{39}\text{Ar}$ geochronology of basement rocks from
19
20 the Mascarene Plateau, the Chagos Bank, and the Maldives Ridge. In: *Scientific Results* (Eds
21
22 R.A. Duncan, J. Backman, and L.C. Peterson), *Proceedings of the Ocean Drilling Program*,
23
24 **115**, 43-51.
25
26

27
28
29
30 Eberli, G.P., Anselmetti, F.S., Isern, A.R. and Delius, H. (2010) Timing of changes in sea-
31
32 level and currents along the Miocene platforms of the Marion Plateau, Australia. In: *Cenozoic*
33
34 *Carbonate Systems of Australasia* (Eds W.A. Morgan, A.D. George, P.M. Harris, J.A. Kupecz
35
36 and J.E. Sarg J.E.), *SEPM Spec. Publ.*, **95**, 219-242.
37
38

39
40
41
42 Hansen, H.J. and Buchardt, B. (1977) Depth distribution of *Amphistegina* in the Gulf of Elat,
43
44 Israel. *Utrecht Micropaleontol. Bull.*, **15**, 205-224.
45
46

47
48
49
50 Hernández-Molina, F.J., Llave, E., Stow, D.A.V. (2008). Continental slope contourites. In:
51
52 *Contourites* (Eds M. Rebesco and A. Camerlenghi), *Dev. Sedimentol.*, **60**, 379-408.
53
54
55
56
57
58
59
60

1
2
3 Hohenegger, J., Yordanova, E., Nakano, Y. and Tatzreiter, F. (1999) Habitats of larger
4 foraminifera on the upper reef slope of Sesoko Island, Okinawa, Japan. *Mar. Micropaleontol.*,
5 **36**, 109-168.
6
7
8
9

10
11
12 Hohenegger, J. (2000) Coenoclines of larger foraminifera. *Micropaleontol.*, **46**, 127-151.
13
14
15
16

17 Hohenegger, J. (1994) Distribution of living larger foraminifera NW of Sesoko Jima,
18 Okinawa, Japan. *Mar. Ecol.*, **15**, 291-334.
19
20
21
22
23
24

25 Huneke, N.V. and Stow, D.A.V. (2008) Identification of ancient contourites: problems and
26 palaeoceanographic significance. In: *Contourites* (Eds M. Rebesco and A. Camerlenghi), *Dev.*
27 *Sedimentol.*, **60**, 323-344.
28
29
30
31
32
33

34 Isern, A., Anselmetti, F.S. and Blum, P. (2004) A Neogene carbonate platform, slope and shelf
35 edifice shaped by sea level and ocean currents, Marion Plateau (Northeast Australia). In:
36 *Seismic imaging of carbonate reservoirs and systems* (Eds G.P. Eberli, J.L. Masferro and J.F.
37 Sarg), *AAPG Mem.*, **81**, 291-307.
38
39
40
41
42
43
44
45

46 John, C.M. and Mutti, M. (2005) The response of heterozoan carbonate systems to
47 Paleooceanographic, climatic and eustatic changes: a perspective from slope sediments of the
48 Marion Plateau (ODP Leg 194). *J. Sed. Res.*, **75**, 51-65.
49
50
51
52
53
54
55
56
57
58
59
60

1
2
3 Lowe, D. R. (1982) Sediment gravity flows: II. Depositional models with special reference to
4 the deposits of high-density turbidity currents. *J. Sed. Petrol.*, **52**, 279-297.
5
6
7

8
9 Lüdmann, T., Kalvelage, C., Betzler, C., Fürstenau, J. and Hübscher, C. (2013) The Maldives,
10 a Giant Isolated Carbonate Platform Dominated by Bottom Currents. *Mar. Petrol. Geol.*, **43**,
11 326-340.
12
13
14
15

16
17
18
19 Lüdmann, T., Paulat, M., Betzler, C., Möbius, J., Lindhorst, S., Wunsch, M. and Eberli, G.P.
20 (2016) Carbonate mounds in the Santaren Channel, Bahamas: a current-dominated
21 periplatform depositional regime. *Mar. Geol.*, **376**, 69-85.
22
23
24
25

26
27
28
29 Lüdmann, T., Betzler, C., Eberli, G.P., Reolid, J., Reijmer, J.J.G., Sloss, C.R., Bialik, O.M.,
30 Alvarez-Zarkikian, C.A., Alonso-Garcia, M., Blatter, C.L., Guo, J.A., Haffen, S., Horozal, S.,
31 Inoue, M., Jovane, L., Kroon, D., Lanci, L., Laya, J.C., Mee, A.L., Nakakuni, M., Nath, B.N.,
32 Niino, K., Petruny, L.M., Pratiwi, S.D., Slagle, A.L., Su, X., Swart, P.K., Wright, J.D., Yao,
33 Z. and Young, J.R. (in press) Carbonate delta drifts: a new drift type. *Mar. Geol.*
34
35
36
37
38
39
40
41

42
43
44 Mateu-Vicens, G., Hallock, P. and Brandano, M. (2009) Test-shape variability of
45 *Amphistegina* d'Orbigny, 1826 as a paleobathymetric proxy: application to two Miocene
46 examples. In: *Geologic Problem Solving with Microfossils: A Volume in Honor of Garry D.*
47 *Jones* (Eds T. Demchuk and A. Gary), *SEPM Spec. Publ.*, **93**, 67-82
48
49
50
51
52

53
54
55 Mitchum, R.M., Vail, P.R. and Sangree, J.B. (1977) Seismic stratigraphy and global changes
56
57
58
59
60

1
2
3 of sea level: Part 6. Stratigraphic interpretation of seismic reflection patterns in depositional
4 sequences. In: *Seismic stratigraphy—applications to hydrocarbon exploration* (Ed C.E.
5 Payton). *AAPG Bull.*, **26**, 117-134.
6
7
8
9

10
11
12 Mulder, T., Syvitski, J.P.M., Migeon, S., Faugères, J.C. and Savoye, B. (2003) Marine
13 hyperpycnal flows: initiation, behavior and related deposits. A review. *Mar. Petrol. Geol.*, **20**,
14 861-882.
15
16
17
18
19

20
21
22 Mullins, H.T. and Neumann, H.C. (1979) Geology of the Miami Terrace and its paleo-
23 oceanographic implications. *Mar. Geol.*, **30**, 205-232.
24
25
26
27
28
29

30
31 Mullins, H.T., Neumann, A.C., Wilber, R.J., Hine, A.C. and Chinburg, A.J. (1980) Carbonate
32 sediment drifts in northern Straits of Florida. *Bull. Am. Assoc. Pet. Geol.*, **64**, 1701-1717.
33
34
35
36
37

38 Neumann, A.C. and Ball, M.M. (1970) Submersible observations in the Straits of Florida:
39 geology and bottom currents. *Geol. Soc. Am. Bull.*, **81**, 2861-2874.
40
41
42
43
44
45

46 Paulat, M., Lüdmann, T., Betzler, C., Eberli, G.P. (submitted) Neogene paleoceanographical
47 changes recorded in a carbonatic contourite drift (Santaren Channel, Bahamas).
48
49
50
51
52
53

54 Purdy, E.G. and Bertram, G.T. (1993) Carbonate Concepts from the Maldives, Indian Ocean.
55
56 AAPG Studies in Geology **34**, 56 pp.
57
58
59
60

1
2
3
4
5
6 Rebesco, M., Hernández-Molina, F.J., Van Rooij, D. and Wåhlin, A. (2014) Contourites and
7 associated sediments controlled by deep-water circulation processes: State-of-the-art and
8 future considerations. *Marine Geology*, **352**, 111-154.
9

10
11
12
13
14
15
16 Renema, W. and Troelstra, S.R. (2001) Larger foraminifera distribution on a mesotrophic
17 carbonate shelf in SW Sulawesi (Indonesia). *Palaeogeogr. Palaeoclimatol. Palaeoecol.*, **175**,
18 125-146.
19
20
21

22
23
24
25 Reolid, J. and Betzler, C. (2018) Ichnofabrics logs for the characterization of the organic
26 content in carbonates. *Marine and Petroleum Geology*.
27 <https://doi.org/10.1016/j.marpetgeo.2018.04.019>
28
29
30
31

32
33
34
35 Reolid, J., Reolid, M., Betzler, C., Lindhorst, S., Wiesner, M. G., Lahajnar, N. (2017) Upper
36 Pleistocene cold-water corals from the Inner Sea of the Maldives: taphonomy and
37 environment, *Facies*, **63**, 1-20.
38
39
40
41

42
43
44 Schnyder, J.S.D., Eberli, G.P., Betzler, C., Wunsch, M., Lindhorst, S., Schiebel, L., Mulder, T.
45 and Ducassou, E. (2018) Morphometric analysis of plunge pools and sediment wave fields
46 along western Great Bahama Bank. *Marine Geology*, **397**, 15-28.
47
48
49
50

51
52
53
54 Stow, D.A.V., Faugères, J.C., Howe, J.A., Pudsey, C.J. and Viana, R. (2002a). Bottom
55 currents, contourites and deep-sea sediment drifts: current state-of-the-art, in: *Deep-Water*
56
57
58
59
60

1
2
3 *Contourite Systems: Modern Drifts and Ancient Series, Seismic and Sedimentary*
4 *Characteristics* (Eds D.A.V. Stow, C.J. Pudsey, J.A. Howe, J.C. Faugères, and A.R. Viana),
5
6
7 *Geol. Soc. London Memoir*, **22**, 7-20.
8
9

10
11
12
13 Stow, D.A.V., Pudsey, C.J., Howe, J.A., Faugères, J. C. and Viana, A.R. (2002b) Deep-Water
14
15 Contourite Systems: Modern Drifts and Ancient Series, Seismic and Sedimentary
16
17 Characteristics. *Geol. Soc. London*, 22, 464 pp.
18
19

20
21
22
23 Stow, D.A.V. and Faugères, J. C. (2008) Contourite facies and the facies model, In:
24
25 *Contourites* (Eds M. Rebesco and A. Camerlenghi), *Dev. Sedimentol.*, **60**, 223-256.
26
27

28
29
30
31 Tsuji, Y. (1993) Tide influenced high energy environments and rhodolith-associated
32
33 carbonate deposition on the outer shelf and slope off the Miyako Islands, southern Ryukyu
34
35 Island Arc, Japan. *Mar. Geol.*, **113**, 255-271.
36
37

38 39 40 41 42 43 44 45 **Figures**

46
47 **Figure 1:** Map of the study area in the northern part of the Maldives (modified after Lüdmann
48
49 et al., 2018). Red box marks the position of B. B) Location of IODP Expedition 359 Sites
50
51 U1465 (drilled in the Miocene carbonate platforms) as well as U1466 and U1468 (drilled in
52
53 the delta drift). Black lines represent the seismic lines displayed in their respective figures.
54
55
56
57
58
59
60

1
2
3 **Figure 2:** West-East overview of the delta drift of the Maldives (modified after Lüdmann et
4 al., 2018). A) Part of reflection seismic line M74-65 that crosses the top of the Middle
5 Miocene carbonate platform and drift delta with location of the IODP Exp. 359 Sites and
6 cross-cutting seismic lines SO236-38 and SO236-23. B) Interpretation with the boundaries of
7 the drift mega-sequences. Drift sequence DS1 is subdivided into subsequences a, b, and c.
8 The study Sites, U1466 and U1468, display the lithological column for the delta drift
9 (shadowed in gray) discussed in text and Figures 6 and 7. Dashed lines exhibit possible fault
10 traces. Arrow heads show reflection terminations.
11
12
13
14
15
16
17
18
19

20 **Figure 3:** West-East overview of the delta drift of the Maldives. A) Part of reflection seismic
21 line SO236-32 that crosses the top of the Middle Miocene carbonate platform and drift delta
22 in a marginal position of the Kardiva Channel. B) Interpretation with the boundaries of the
23 drift mega-sequences (yellow shadowed), and subsequences of ds1. The studied interval of
24 the delta drift is white and carbonate platform slope deposits are blue shadowed. Arrow heads
25 show reflection terminations.
26
27
28
29
30
31
32

33 **Figure 4:** North-South overview of the delta drift of the Maldives at the position of Site
34 U1466. A) Part of reflection seismic line SO236-38. B) Interpretation with the boundaries of
35 the drift mega-sequences (yellow shadowed), and subsequences of ds1. The studied interval
36 of the delta drift is white and includes the lithological column. Carbonate platform slope
37 deposits are blue shadowed. Arrow heads show reflection terminations.
38
39
40
41
42
43

44 **Figure 5:** North-South overview of the delta drift of the Maldives at the position of Site
45 U1468. A) Part of reflection seismic line SO236-23. B) Interpretation with the boundaries of
46 the drift mega-sequences (yellow shadowed), and subsequences of ds1. The studied interval
47 of the delta drift is white and includes the lithological column. Carbonate platform slope
48 deposits are blue shadowed. Arrow heads show reflection terminations.
49
50
51
52
53

54 **Figure 6:** Lithological column of the delta drift at Site U1466 including from left to right:
55 depth (mbsf), core, recovery, core photographs, sequence boundary, carbonate texture, grain
56
57
58
59
60

1
2
3 size, gamma radiation (HSGR, NGR, and spectral gamma radiation for uranium),
4 components, position of the thin sections, and reflexion-seismic profile.
5
6

7 **Figure 7:** Lithological column of the delta drift at Site U1468 including from left to right:
8 depth (mbsf), core, recovery, core photographs, sequence boundary, carbonate texture, grain
9 size, gamma radiation (HSGR, NGR), main facies components, position of the thin sections,
10 and reflexion-seismic profile.
11
12
13
14

15 **Figure 8:** Photomicrographs of representative facies of the delta drift. **A)** Foraminiferal
16 packstone with abundant planktonic foraminifera and pellets and minor *Cycloclypeus* (C) and
17 *Miogypsina* (M) at U1466 (279.36 mbsf). **B)** Fine-grained bioclastic packstone at U1466
18 (222.13 mbsf). **C)** *Cycloclypeus* wackestone with planktonic foraminifera and flattened forms of
19 *Cycloclypeus* at U1466 (162.88). **D)** Fragmented LBF packstone with *Amphistegina* (A) and
20 broken pieces of *Cycloclypeus* at U1466 (114.06 mbsf). **E)** Nummulitid packstone with
21 *Lepidocyclina* (L) and abundant *Cycloclypeus* at U1466 (117.11 mbsf). **F)** *Amphistegina*
22 grainstone with abundant *Amphistegina* and red algae fragments (R) at U1468 (143.15 mbsf).
23
24
25
26
27
28
29
30
31

32 **Figure 9:** Main facies of the delta drift at Site U1468. **A)** Photomicrograph of the sponge
33 spicule-bryozoan wackestone to packstone (305.80 mbsf). **B)** Photomicrograph of the chert-
34 nodule packstone with abundant pellets (301.10 mbsf). **C)** Photomicrograph of the
35 *Lepidocyclina* packstone with abundant *Lepidocyclina* (L) and *Amphistegina* (A) (164.10
36 mbsf). **D)** Photomicrograph of the *Halimeda* grainstone with partially dissolved *Halimeda*
37 plates (H), red algae fragments (R), *Amphistegina*, *Cycloclypeus* (C), and equinoid remains
38 (E) (78.58 mbsf). **E)** Core photograph of an *Amphistegina* rudstone to grainstone with
39 abundant intraclasts (I), echinoid fragments, and diverse large benthic foraminifera (127.19
40 mbsf). This facies shows fining-upward grading that consists of 3-cm-thick interval of gravel
41 to granule materials (especially intraclasts) that grades upward into a 10-cm-thick interval
42 ranging from gravel at the base to fine-grained carbonate sand to the top. The top of this
43 interval is eroded by the next interval of fining.
44
45
46
47
48
49
50
51
52
53
54
55
56
57
58
59
60

1
2
3 **Figure 10:** Evolution of the delta drift of the Maldives. In the first stage the deposition was in
4 a current-controlled deep environment. Progressively the accommodation space is infilled at
5 the proximal part of the delta drift that is progressively colonized by shallow-water biota. The
6 distal areas of the drift are less productive and the deposition there is dominated by currents
7 and pelagic settling. Black arrows represent dominant bottom currents.
8
9
10
11
12

13 **Figure 11:** Conceptual diagram after Rebesco et al. (2014) showing the four main types of
14 sedimentary processes operating in carbonate drifts (see discussion in text). The base triangle
15 represents the factors controlling siliciclastic drifts (Rebesco et al., 2014) and also deep-water
16 carbonate drifts. The upper vertex of the pyramid represents the shallow water regime. Every
17 depositional environment where drifts may occur, including the delta drift, is comprised
18 within this pyramid.
19
20
21
22
23
24
25
26
27
28
29
30
31
32
33
34
35
36
37
38
39
40
41
42
43
44
45
46
47
48
49
50
51
52
53
54
55
56
57
58
59
60

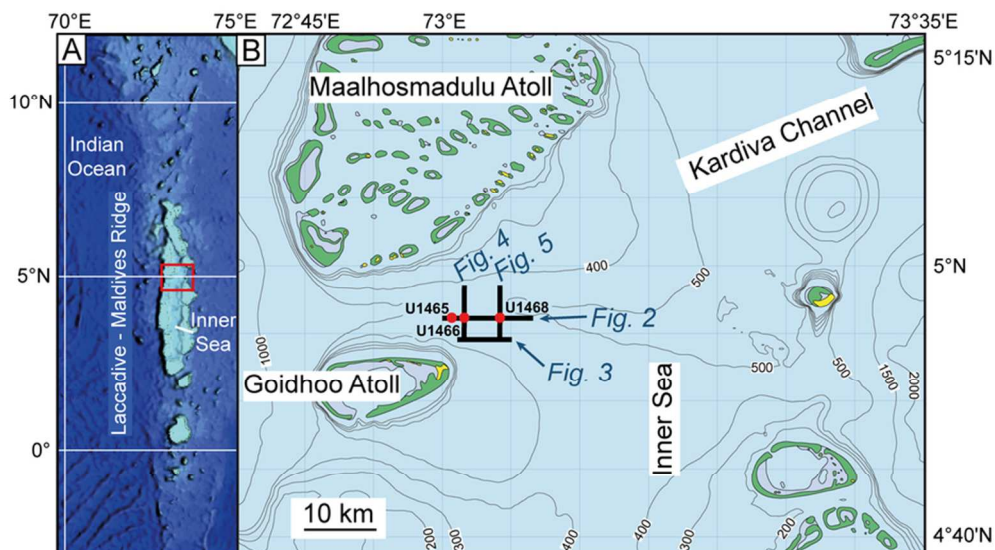


Figure 1: Map of the study area in the northern part of the Maldives (modified after Lüdmann et al., 2018). Red box marks the position of B. B) Location of IODP Expedition 359 Sites U1465 (drilled in the Miocene carbonate platforms) as well as U1466 and U1468 (drilled in the delta drift). Black lines represent the seismic lines displayed in their respective figures.

79x44mm (300 x 300 DPI)

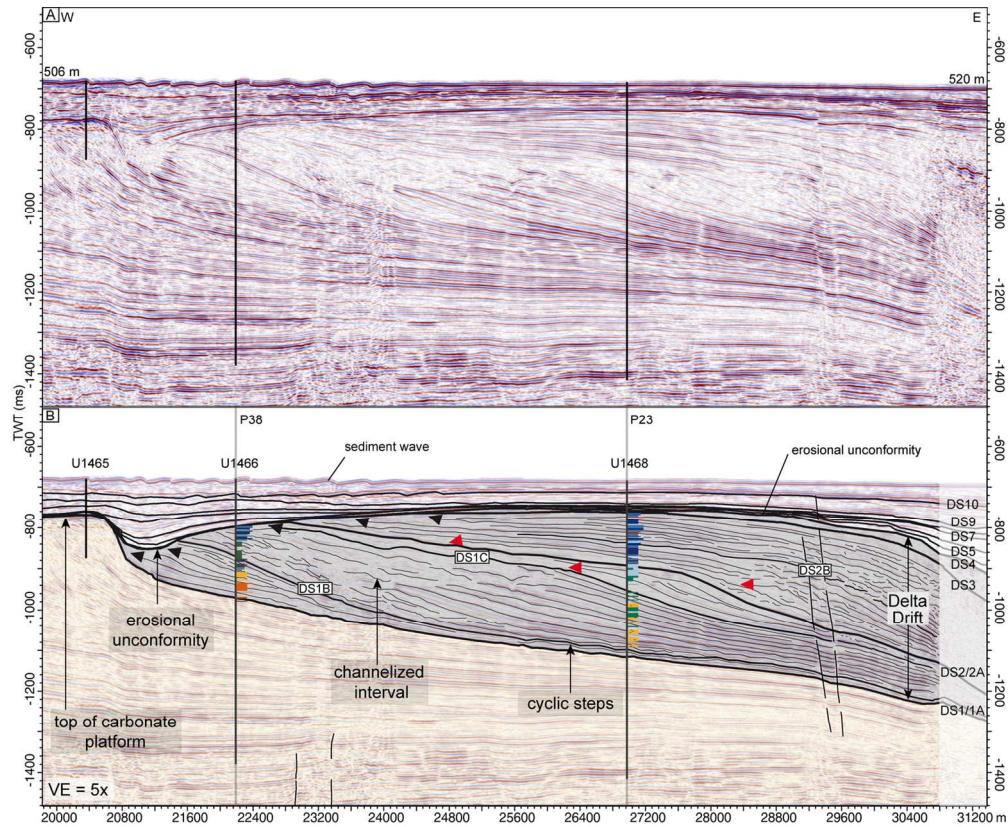


Figure 2: West-East overview of the delta drift of the Maldives (modified after Lüdmann et al., 2018). A) Part of reflection seismic line M74-65 that crosses the top of the Middle Miocene carbonate platform and drift delta with location of the IODP Exp. 359 Sites and cross-cutting seismic lines SO236-38 and SO236-23. B) Interpretation with the boundaries of the drift mega-sequences. Drift sequence DS1 is subdivided into subsequences a, b, and c. The study Sites, U1466 and U1468, display the lithological column for the delta drift (shaded in gray) discussed in text and Figures 6 and 7. Dashed lines exhibit possible fault traces. Arrow heads show reflection terminations.

136x111mm (300 x 300 DPI)

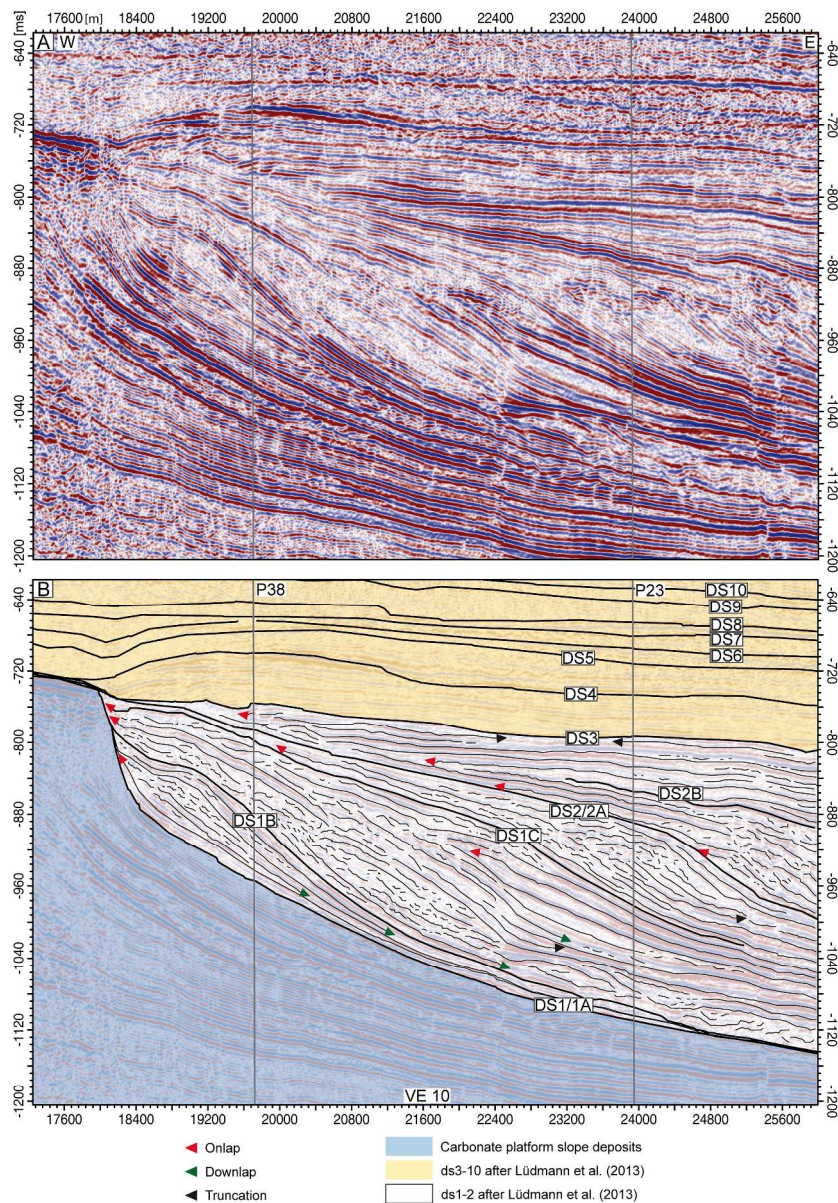


Figure 3: West-East overview of the delta drift of the Maldives. A) Part of reflection seismic line SO236-32 that crosses the top of the Middle Miocene carbonate platform and drift delta in a marginal position of the Kardiva Channel. B) Interpretation with the boundaries of the drift mega-sequences (yellow shadowed), and subsequences of ds1. The studied interval of the delta drift is white and carbonate platform slope deposits are blue shadowed. Arrow heads show reflection terminations.

256x366mm (300 x 300 DPI)

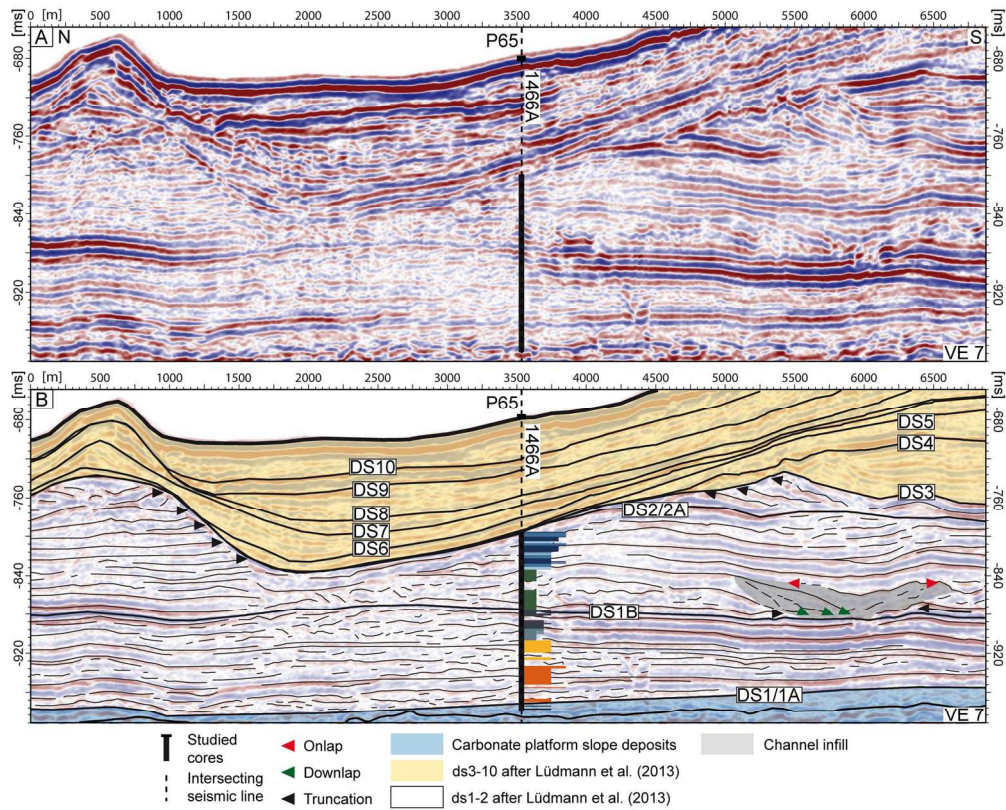


Figure 4: North-South overview of the delta drift of the Maldives at the position of Site U1466. A) Part of reflection seismic line SO236-38. B) Interpretation with the boundaries of the drift mega-sequences (yellow shadowed), and subsequences of ds1. The studied interval of the delta drift is white and includes the lithological column. Carbonate platform slope deposits are blue shadowed. Arrow heads show reflection terminations.

154x124mm (300 x 300 DPI)

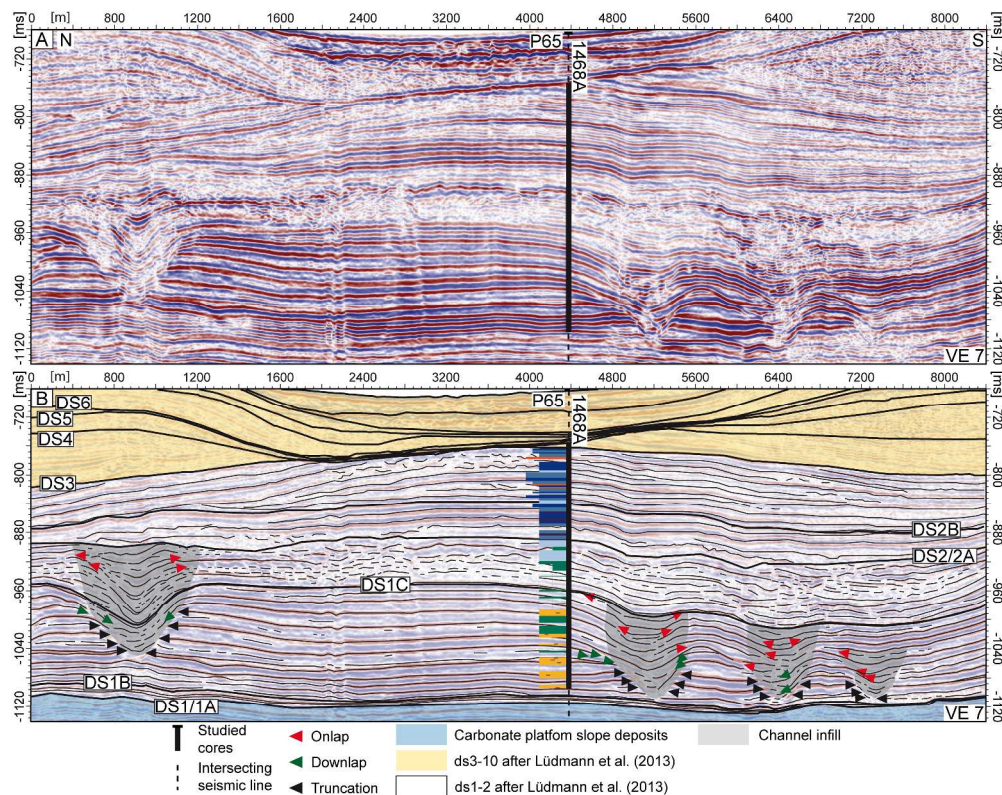


Figure 5: North-South overview of the delta drift of the Maldives at the position of Site U1468. A) Part of reflection seismic line SO236-23. B) Interpretation with the boundaries of the drift mega-sequences (yellow shadowed), and subsequences of ds1. The studied interval of the delta drift is white and includes the lithological column. Carbonate platform slope deposits are blue shadowed. Arrow heads show reflection terminations.

197x157mm (500 x 500 DPI)

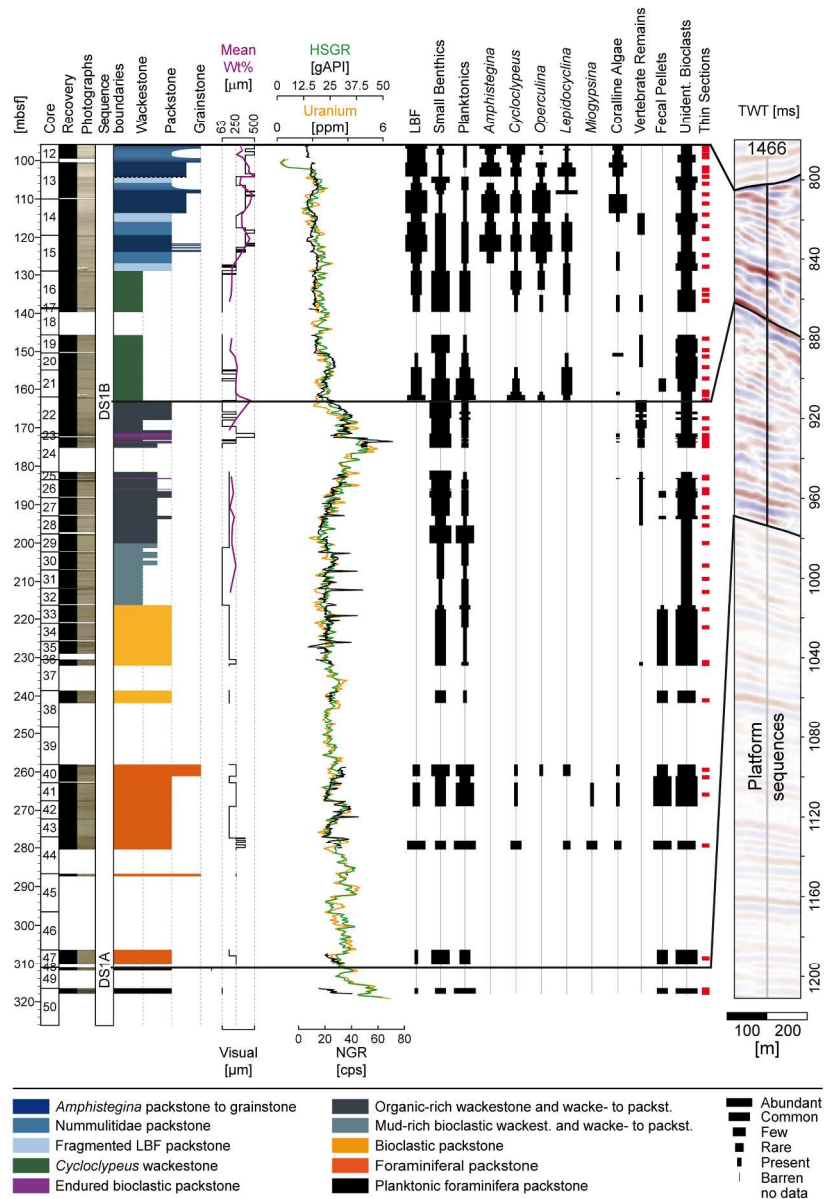


Figure 6: Lithological column of the delta drift at Site U1466 including from left to right: depth (mbsf), core, recovery, core photographs, sequence boundary, carbonate texture, grain size, gamma radiation (HSGR, NGR, and spectral gamma radiation for uranium), components, position of the thin sections, and reflection-seismic profile.

207x297mm (300 x 300 DPI)

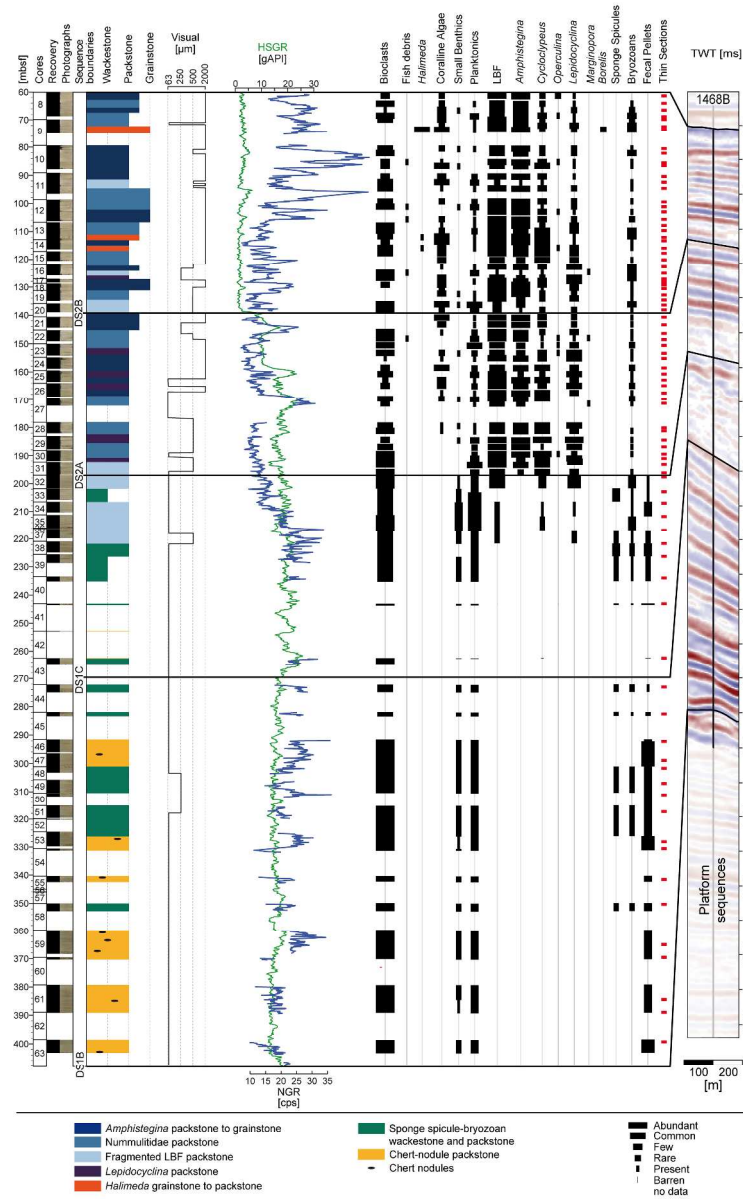


Figure 7: Lithological column of the delta drift at Site U1468 including from left to right: depth (mbsf), core, recovery, core photographs, sequence boundary, carbonate texture, grain size, gamma radiation (HSGR, NGR), main facies components, position of the thin sections, and reflexion-seismic profile.

283x445mm (300 x 300 DPI)

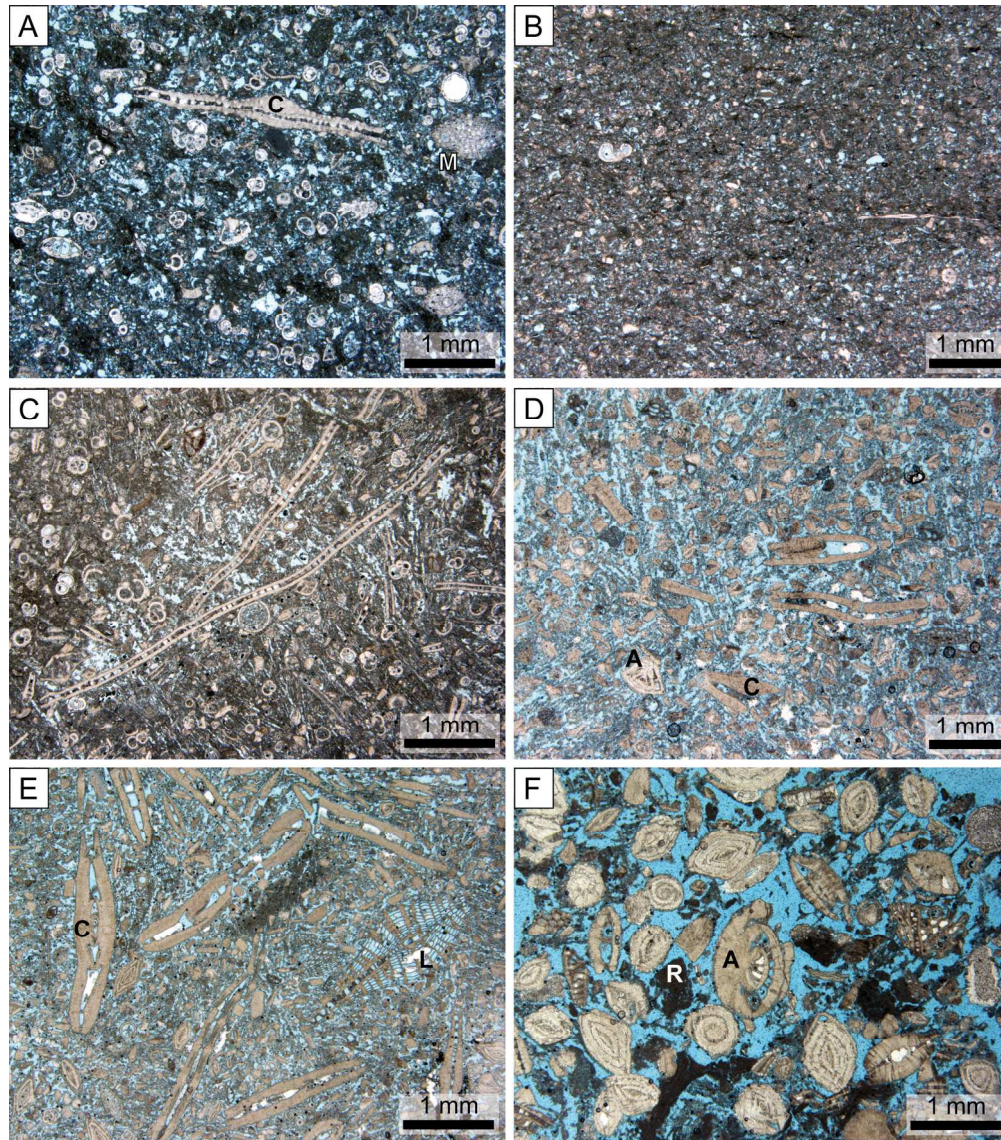


Figure 8: Photomicrographs of representative facies of the delta drift. A) Foraminiferal packstone with abundant planktonic foraminifera and pellets and minor *Cycloclypeus* (C) and *Miogypsina* (M) at U1466 (279.36 mbsf). B) Fine-grained bioclastic packstone at U1466 (222.13 mbsf). C) *Cycloclypeus* wackestone with planktonic foraminifera and flattened forms of *Cycloclypeus* at U1466 (162.88). D) Fragmented LBF packstone with *Amphistegina* (A) and broken pieces of *Cycloclypeus* at U1466 (114.06 mbsf). E) Nummulitid packstone with *Lepidocyclina* (L) and abundant *Cycloclypeus* at U1466 (117.11 mbsf). F) *Amphistegina* grainstone with abundant *Amphistegina* and red algae fragments (R) at U1468 (143.15 mbsf).

173x196mm (300 x 300 DPI)

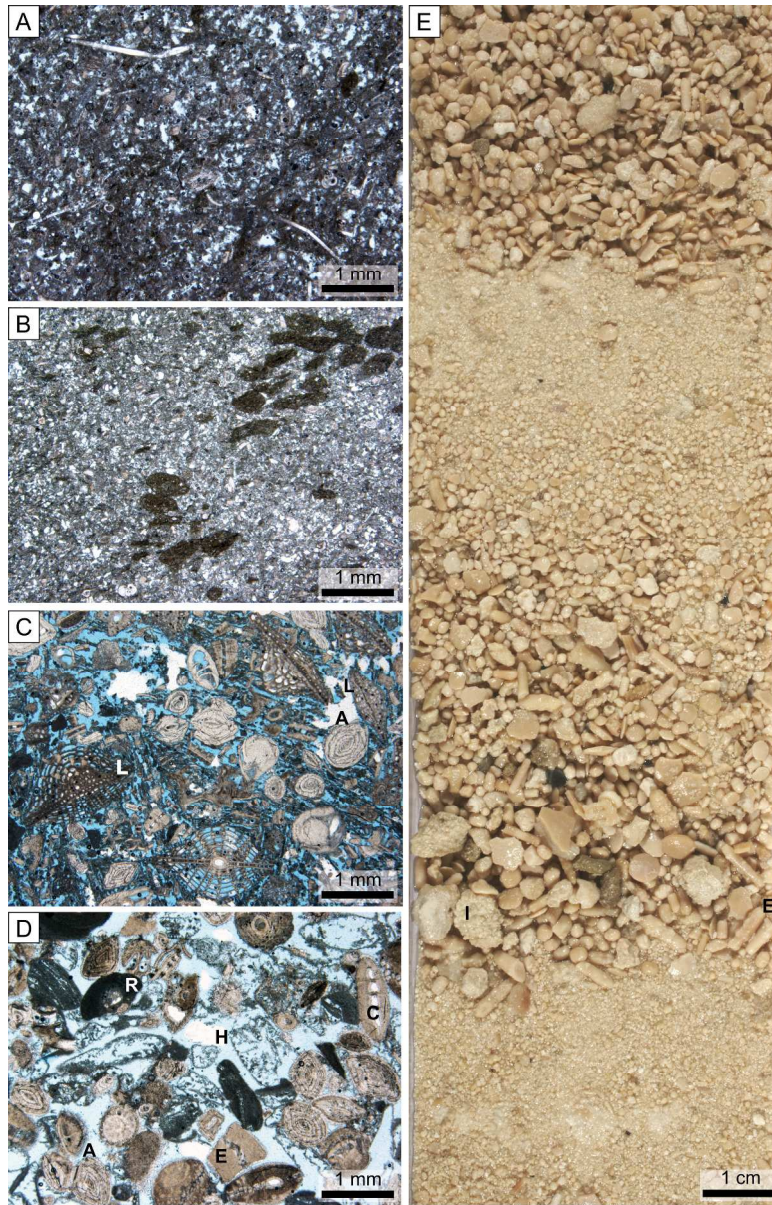


Figure 9: Main facies of the delta drift at Site U1468. A) Photomicrograph of the sponge spicule-bryozoan wackestone to packstone (305.80 mbsf). B) Photomicrograph of the chert-nodule packstone with abundant pellets (301.10 mbsf). C) Photomicrograph of the *Lepidocyclina* packstone with abundant *Lepidocyclina* (L) and *Amphistegina* (A) (164.10 mbsf). D) Photomicrograph of the *Halimeda* grainstone with partially dissolved *Halimeda* plates (H), red algae fragments (R), *Amphistegina*, *Cycloclypeus* (C), and equinoid remains (E) (78.58 mbsf). E) Core photograph of an *Amphistegina* rudstone to grainstone with abundant intraclasts (I), echinoid fragments, and diverse large benthic foraminifera (127.19 mbsf). This facies shows fining-upward grading that consists of 3-cm-thick interval of gravel to granule materials (especially intraclasts) that grades upward into a 10-cm-thick interval ranging from gravel at the base to fine-grained carbonate sand to the top. The top of this interval is eroded by the next interval of fining.

230x358mm (300 x 300 DPI)

1
2
3
4
5
6
7
8
9
10
11
12
13
14
15
16
17
18
19
20
21
22
23
24
25
26
27
28
29
30
31
32
33
34
35
36
37
38
39
40
41
42
43
44
45
46
47
48
49
50
51
52
53
54
55
56
57
58
59
60

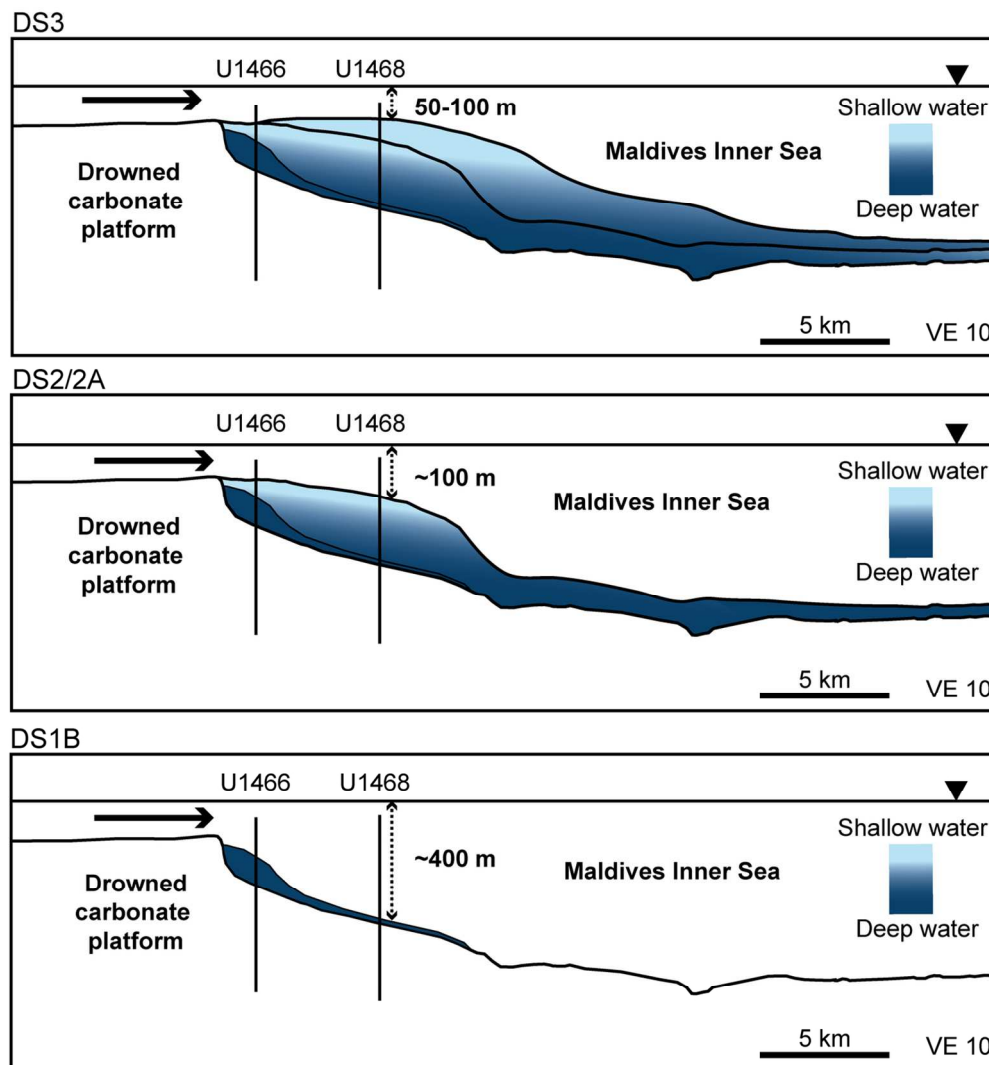


Figure 10: Evolution of the delta drift of the Maldives. In the first stage the deposition was in a current-controlled deep environment. Progressively the accommodation space is infilled at the proximal part of the delta drift that is progressively colonized by shallow-water biota. The distal areas of the drift are less productive and the deposition there is dominated by currents and pelagic settling. Black arrows represent dominant bottom currents.

126x135mm (300 x 300 DPI)

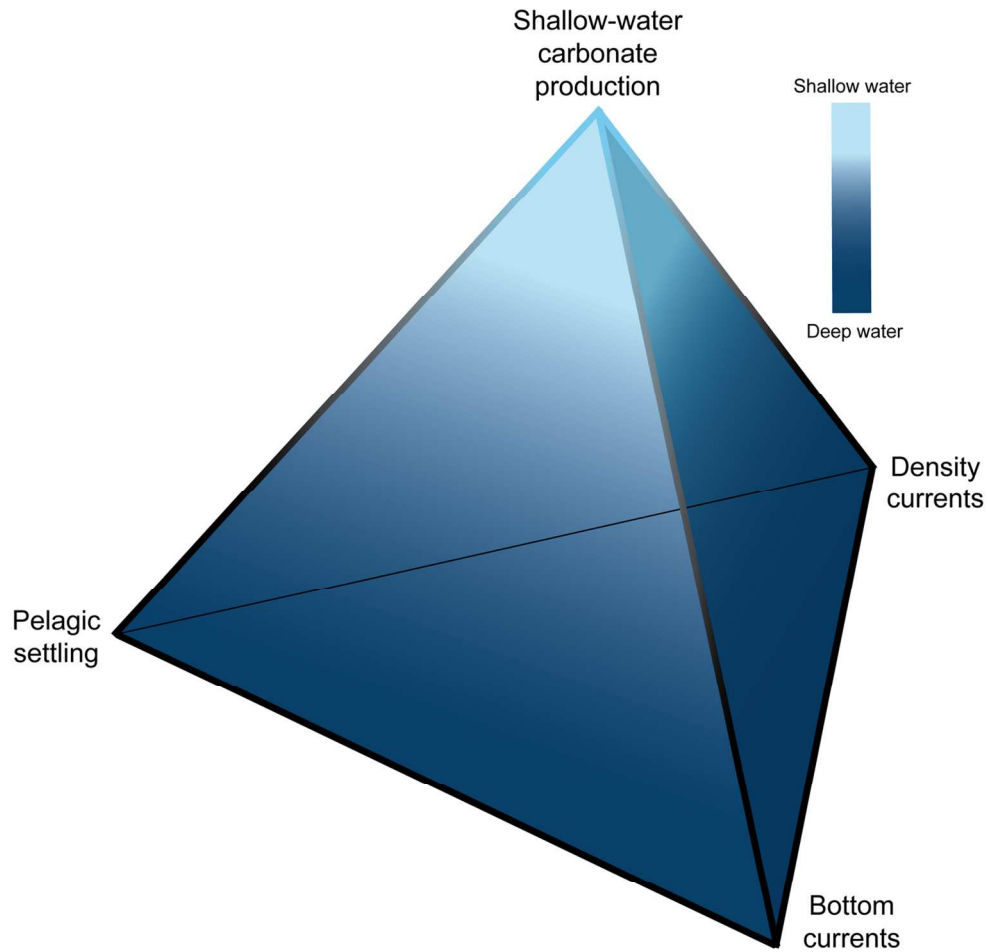


Figure 11: Conceptual diagram after Rebesco et al. (2014) showing the four main types of sedimentary processes operating in carbonate drifts (see discussion in text). The base triangle represents the factors controlling siliciclastic drifts (Rebesco et al., 2014) and also deep-water carbonate drifts. The upper vertex of the pyramid represents the shallow water regime. Every depositional environment where drifts may occur, including the delta drift, is comprised within this pyramid.

127x124mm (300 x 300 DPI)

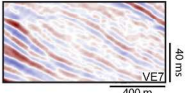
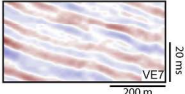
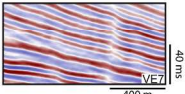
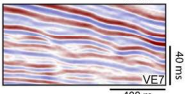
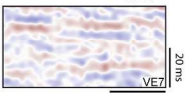
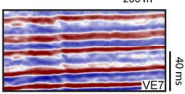
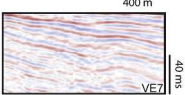
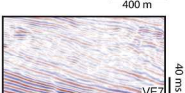
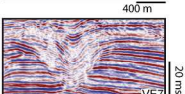
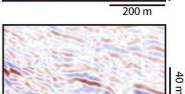
| Seismic facies | Illustration | Reflection configuration | Amplitude/continuity | Subsequence | Microfacies |
|----------------|---|---------------------------------------|---|------------------|--|
| SF1 |  | Sigmoid progradational to subparallel | Low to Medium | ds1a | Foraminiferal packstone, Bioclastic packstone, Mud-rich bioclastic wackestone-packstone, organic-rich wackestone |
| SF2 |  | Parallel to subparallel | Low to medium/medium to high | ds1a, ds1b | Not drilled. Transitional from LBF-rich facies to the facies rich in spicules and chert nodules |
| SF3 |  | Parallel, even | High/high | ds1b, ds1c | Sponge spicule wackestone to packstone, Chert nodule packstone |
| SF4 |  | Wavy (cyclic steps) | Medium to high/medium to high | ds1a | Poor recovery, fine-grained bioclastic packstone? |
| SF5 |  | Subparallel, hummocky | Low to medium. Laterally grades into SF6 | ds1, ds2 | Foraminiferal packstone, Bioclastic packstone, Cycloclypeus wackestone, Halimeda grainstone, LBF-rich facies |
| SF6 |  | Parallel | Medium to high. Laterally grades into SF5 and SF9 | ds1, ds2 | Sponge spicule wackestone to packstone, Chert nodule packstone, and some LBF-rich facies |
| SF7 |  | Sigmoid, subparallel, divergent | Low to medium. Basinwards grades into SF8 | ds1c, ds2a, ds2b | Not drilled. Probably LBF-rich facies |
| SF8 |  | Large sigmoid, convergent | Medium to low | ds1c, ds2a, | Not drilled. Probably LBF-rich facies |
| SF9 |  | Channelized, truncated, disrupted | High to medium | ds1b, ds1c | Not drilled. Probably fine-grained materials to the channel margins and LBF in the center |
| SF10 |  | Chaotic, disrupted | Low to medium/low to medium | ds1b, ds1c | E-W visualization of the channelized facies. Likely LBF-rich facies |

Table 1: Summary of the main features of the seismic facies.

247x284mm (300 x 300 DPI)

| Name | Grain size, sorting, and texture | Major components | Minor Components | Preservation of the components | Matrix | Sedimentary structures |
|-----------------------------------|--|---|---|---|--|--|
| Planktonic foraminifera packstone | Fine-grained packstone. | Unidentifiable bioclasts, planktonic and benthic foraminifera. | Echinoid spines, fecal pellets, and mollusks. | Mollusks are fragmented. | Micrite. | Completely bioturbated. |
| Foraminiferal packstone | Poor- to medium-sorted, silt- to pebble-sized packstone to floatstone. | Unidentifiable bioclasts and planktonic foraminifera. Locally LBF are common. | Mollusks, bryozoans, benthic foraminifera, encrusting foraminifera, red algae, and LBF (<i>Cycloclypeus</i> , <i>Lepidocyclina</i> , <i>Miogypsina</i> , and <i>Nummulites</i>). | Mollusks and LBF are fragmented. Discoidal LBF (<i>Cycloclypeus</i> and <i>Operculina</i>) are mostly fragmented. | Microgranular with minor micrite. | Completely bioturbated. |
| Bioclastic packstone | Well-sorted, fine grained packstone. | Unidentifiable bioclasts, planktonic and benthic foraminifera, and fecal pellets. | Echinoid spines. | Fecal pellets are deformed by compaction. | Microgranular with minor matrix. | Completely bioturbated. |
| Mud-rich bioclastic wackestone | Well-sorted, mud-rich wackestone to packstone. | Unidentifiable bioclasts, benthic and planktonic foraminifera. | Echinoid spines. | The bioclasts are extensively fragmented. | Micrite. | Completely bioturbated. |
| Organic-rich wackestone | Medium-sorted, fine-to-medium grained wackestone to packstone. | Unidentifiable bioclasts and benthic foraminifera. | Planktonic foraminifera, equinoid spines, fecal pellets, vertebrate remains and particulate organic matter. Red algae and brachiopods are present in indurated intervals. | Vertebrate remains occur as fragments of up to 500 μm , locally with celestine overgrowths. | Micritic and minor microgranular. | Completely bioturbated. Locally, celestine nodules of up to 2 cm occur. There are centimeter- to meter-thick indurated intervals alternating with the background facies. |
| <i>Cycloclypeus</i> wackestone | Bimodal sorting, silt and medium-sand sized wackestone. | LBF (<i>Cycloclypeus</i> , <i>Lepidocyclina</i> , and <i>Operculina</i>), planktonic foraminifera and unidentifiable bioclasts. | Benthic and encrusting foraminifera, echinoid spines, <i>Nummulites</i> , mollusks, and red algae nodules. | Minor fragmentation, mostly in mollusks. | Micrite. | Completely bioturbated. |
| Fragmented LBF packstone | Bimodal sorting, silt and medium-sand sized packstone. | Unidentifiable bioclasts and LBF (<i>Amphistegina</i> , <i>Cycloclypeus</i> , <i>Operculina</i> , and <i>Lepidocyclina</i>). | Red algae, equinoid spines, mollusks, and planktonic foraminifera. Red algae are branched and nodular. Benthic foraminifera, bryozoans, and sponge spicules occur in distal settings. | Fragmentation is abundant. LBF fragments are angular, and unidentifiable bioclasts are mostly rounded. | Microgranular with minor amounts of micrite. | Bioturbated (drilling disturbance prevents specification). |
| Nummulitid | Poorly sorted, | LBF (<i>Amphistegina</i> , | Planktonic foraminifera, | Bivalves, red algae, and | Microgranular. | Completely bioturbated. |

| | | | | | | | |
|----|------------------------------------|--|---|---|---|---|---|
| 5 | packstone. | coarse grained packstone. | <i>Cycloclypeus</i> , <i>Operculina</i> , and <i>Lepidocyclina</i>), and unidentifiable bioclasts. | bryozoans, red algae, equinoid spines, and bivalves. Red algae occur as nodules or as crust over other bioclasts. | LBF are fragmented. <i>Cycloclypeus</i> and <i>Operculina</i> are thin walled, and fragmented to a minor degree. | | This facies show gradual and erosive contacts with the <i>Amphistegina</i> packstone. |
| 9 | <i>Amphistegina</i> packstone. | Very poorly-sorted, coarse grained packstone to grainstone (rudstone). | LBF (<i>Amphistegina lessonii</i> , <i>Amphistegina lobifera</i> , <i>Cycloclypeus</i> , <i>Operculina</i> , <i>Lepidocyclina</i>) and nodular and encrusting red algae up to 5 mm in size. | Echinoid spines, bryozoans, gastropods, bivalves and rarely planktonic foraminifera. Intraclasts are locally abundant. | Most of the bioclast are fragmented and have angular shapes. <i>Cycloclypeus</i> and <i>Operculina</i> are flatted, thin walled, and extensive fragmented. <i>Amphistegina</i> individuals are rarely fragmented. | Microgranular and minor micrite. | Completely bioturbated. Intervals with abundant <i>Lepidocyclina</i> are micrite rich. There are bigradational intervals and gradual and erosive contacts between the grainstone and packstone intervals. |
| 17 | Chert-nodule packstone. | Medium-sorted, very fine grained packstone. | Unidentifiable bioclasts and fecal pellets. | Planktonic and benthic foraminifera, and echinoid spines. Chert nodules up to several centimeters in size occur. | Pellets may be locally compacted and accumulated in burrows. | Micrite. | Completely bioturbated. |
| 21 | Sponge spicule-bryozoan packstone. | Medium-sorted, very fine-grained wackestone to packstone. | Unidentifiable bioclasts, sponge spicules (mono axon and triaxon) and bryozoans. | Planktonic and benthic foraminifera, fecal pellets, and echinoid spines. | Bryozoans occur as coarse sand fragments. | Micrite. | Completely bioturbated. |
| 25 | <i>Lepidocyclina</i> packstone. | Very poorly-sorted, coarse grained packstone to grainstone (floatstone). | LBF (<i>Lepidocyclina</i> , <i>Amphistegina</i> , <i>Cycloclypeus</i>) and nodular and encrusting red algae up to 5 mm in size. | Echinoid spines, bryozoans, and rarely planktonic foraminifera. | Most of the bioclast are fragmented and have angular shapes. <i>Cycloclypeus</i> are flatted, thin walled, and extensive fragmented. <i>Amphistegina</i> individuals are rarely fragmented. | Microgranular and minor micrite. | Completely bioturbated. There are gradual and erosive contacts between the <i>Lepidocyclina</i> packstone and other LBF-rich facies. |
| 32 | <i>Halimeda</i> grainstone. | Poorly sorted, coarse grained grainstone to packstone (rudstone). | LBF (<i>Amphistegina</i> , and minor <i>Cycloclypeus</i> , <i>Lepidocyclina</i> , and <i>Operculina</i>), <i>Halimeda</i> plates, and nodular and encrusting red algae up to 5 mm in size. | Echinoid spines, <i>Borelis</i> , bryozoans, encrusting foraminifera, and rarely planktonic foraminifera. Intraclasts are abundant. | Most of the bioclast are fragmented and have angular shapes. <i>Halimeda</i> are partially dissolved. | Absent. When present it is microgranular. | Massive. None sedimentary structures observed. Contacts with other facies may be gradual or erosive. |

Table 2: Summary of the main features of the delta drift facies.